[PS]Quantifying Effective Porosity of Oil and Gas Reservoirs*

(Max) Qinhong Hu[1]

Search and Discovery Article #70376 (2018)**
Posted December 17, 2018

*Adapted from poster presentation given at 2018 International Conference and Exhibition, Cape Town, South Africa, November 4-7, 2018
 DOI:10.1306/70376Hu2018

[1]University of Texas at Arlington, Arlington, TX, United States (maxhu@uta.edu)

Abstract

Microscopic pore structure characteristics of oil and gas reservoirs (e.g., sandstones, carbonates, and mudrocks) – pore shape, pore-size distribution, and pore connectivity – control fluid flow and hydrocarbon movement. Focusing on effective porosity, the portion of connected pore space as conductive pathways to participate in flow and movement ($\emptyset_e$ / $\emptyset$, as an indicator of macroscopic connectivity), this presentation discusses various approaches to quantifying effective porosity for a range of oil and gas reservoirs. The approaches include pycnometry (liquid and gas), pore and bulk volume measurement after vacuum saturation, porosimetry (mercury injection capillary pressure, low-pressure gas physisorption isotherm, water vapor adsorption/desorption isotherm, nuclear magnetic resonance cyroporometry), imaging (X-ray computed tomography, Wood's metal impregnation, field emission-scanning electron microscopy), scattering (ultra- and small-angle neutron, small-angle X-ray), and the utility of both hydrophilic and hydrophobic fluids as well as fluid invasion tests (imbibition, diffusion, vacuum saturation) followed by laser ablation-inductively coupled plasma-mass spectrometry imaging of different nm-sized tracers. Our results indicate disparate characteristics and range of effective porosity, with a single-zone behavior and a value of connectivity at approximately 70% for sandstones, as compared to dual-connectivity zones at 70% and 0.01% for mudrocks.

Selected References

David, C., J. Wassermann, F. Amann, D.A. Lockner, E.H. Rutter, T. Vanorio, A. Amann-Hildenbrand, J. Billiotte, T. Reuschlé, D. Lasseux, J. Fortin, R. Lenormand, A.P.S. Selvadurai, P.G. Meredith, J. Browning, T.M. Mitchell, D. Loggia, F. Nono, J. Sarout, L. Esteban, C. Davy, L. Louis, G. Boitnott, C. Madonna, E. Jahns, M. Fleury, G. Berthe, P. Delage, P. Braun, D. Grégoire, L. Perrier, P. Polito, Y. Jannot, A. Sommier, B. Krooss, R. Fink, Q. Hu, J. Klaver, and A. Clark, 2018, KG²B, A Collaborative Benchmarking Exercise for Estimating the Permeability of the Grimsel Granodiorite – Part 1: Measurements, Pressure Dependence, and Pore-Fluid Effects: *Geophysical Journal International*, v. 215/2, p. 799-824. doi.org/10.1093/gji/ggy304

David, C., J. Wassermann, F. Amann, J. Klaver, C. Davy, J. Sarout, L. Esteban, E.H. Rutter, Q. Hu, L. Louis, P. Delage, D.A. Lockner, A.P.S. Selvadurai, T. Vanorio, A. Amann-Hildenbrand, P.G. Meredith, J. Browning, T.M. Mitchell, C. Madonna, J. Billiotte, T. Reuschlé, D. Lasseux,

J. Fortin, R. Lenormand, D. Loggia, F. Nono, G. Boitnott, E. Jahns, M. Fleury, G. Berthe, P. Braun, D. Grégoire, L. Perrier, P. Polito, Y. Jannot, A. Sommier, B. Krooss, R. Fink, and A. Clark; KG²B, A Collaborative Benchmarking Exercise for Estimating the Permeability of the Grimsel Granodiorite - Part 2: Modelling, Microstructures, and Complementary Data: *Geophysical Journal International*, v. 215,/2, p. 825-843. doi.org/10.1093/gji/ggy305

Gao, Z.Y., and Q.H. Hu, 2018, Pore Structure and Spontaneous Imbibition of Marine and Continental Shales in China: American Association of Petroleum Geologist Bulletin, v. 102/10, p. 1941-1961.

Gao, Z.Y., and Q.H. Hu, 2016, Wettability of Mississippian Barnett Samples at Different Depths: Investigations from Directional Spontaneous Imbibition: American Association of Petroleum Geologist Bulletin, v. 100/1, p. 101-114.

Gao, Z.Y., and Q.H. Hu, 2013, Estimating Permeability Using Median Pore-Throat Radius Obtained from Mercury Intrusion Porosimetry: Journal of Geophysics and Engineering, v. 10, p. 025014.

Hager, J., 1998, Steam Drying of Porous Media: Ph.D. Thesis, Department of Chemical Engineering, Lund University, Sweden.

Hu, Q.H., T.J. Kneafsey, J.S.Y. Wang, L. Tomutsa, and J.J. Roberts, 2004, Characterizing Unsaturated Diffusion in Porous Tuff Gravels: Vadose Zone Journal, v. 3/4, p. 1425-1438.

Hu, Q.H., R.P. Ewing, and S. Dultz, 2012, Pore Connectivity in Natural Rock: Journal of Contaminant Hydrology, v. 133, p. 76-83.

Hu, Q.H., and X.L. Mao, 2012, Applications of Laser Ablation-Inductively Coupled Plasma-Mass Spectrometry in Studying Chemical Diffusion, Sorption, and Transport in Natural Rock: Geochemical Journal, v. 46/5, p. 459-475.

Hu, Q.H., R.P. Ewing, and H.D. Rowe, 2015, Low Nanopore Connectivity Limits Gas Production in Barnett Formation: Journal of Geophysical Research – Solid Earth, v. 120/12, p. 8073-8087.

Hu, Q.H., H. Liu, R. Yang, Y.X. Zhang, G. Kibria, S. Sahi, N. Alatrash, F.M. MacDonnell, and W. Chen, 2017, Applying Molecular and Nanoparticle Tracers to Study Wettability and Connectivity of Longmaxi Formation in Southern China: Journal of Nanoscience and Nanotechnology, v. 17, p. 6284-6295.

Hu, Q.H., Y.X. Zhang, X.H. Meng, Z. Li, Z.H. Xie, and M.W. Li, 2017, Characterization of Multiple Micro-Nano Pore Networks in Shale Oil Reservoirs of Paleogene Shahejie Formation in Dongying Sag of Bohai Bay Basin, East China: Petroleum Exploration and Development, v. 44/5, p. 720-730.

Hu, Q.H., W. Zhou, P. Huggins, and W.L. Chen, 2018, Pore Structure and Fluid Uptake of the Goddard Shale Formation in Southeastern Oklahoma, USA: Geofluids, Article ID 5381735.

Katz, A.J., and A.H. Thompson, 1986, Quantitative Prediction of Permeability in Porous Rock: Physical Review B, v. 34, p. 8179-8181.

Katz, A.J., and A.H. Thompson, 1987, Prediction of Rock Electrical Conductivity from Mercury Injection Measurements: Journal of Geophysical Research, v. 92/B1, p. 599-607.

Kaufmann, J., 2010, Pore Space Analysis of Cement-Based Materials by Combined Nitrogen Sorption - Wood's Metal Impregnation and Multi-Cycle Mercury Intrusion: Cement and Concrete Composites, v. 32/7, p. 514-522.

Norton, D., and R. Knapp, 1977, Transport Phenomena in Hydrothermal Systems: Nature of Porosity: American Journal of Science, v. 27, p. 913-936.

Washburn, E.W., 1921, Note on a Method of Determining the Distribution of Pore Sizes in a Porous Material: Proceeding of the National Academy of Science U.S.A., v. 7, p. 115-116.

Zhao, J.H., Z.J. Jin, Q.H. Hu, Z.K. Jin, T.J. Barber, Y.X. Zhang, and M.K. Bleuel, 2017, Integrating SANS and Fluid-Invasion Methods to Characterize Pore Structure of Typical American Shale Oil Reservoirs: Scientific Reports, v. 7, p. 15413.

Quantifying effective porosity of oil and gas reservoirs

UNIVERSITY OF TEXAS ARLINGTON

(Max) Qinhong Hu (*maxhu@uta.edu*), The University of Texas at Arlington, Arlington, TX 76019

Introduction

- Microscopic pore structure characteristics of oil and gas reservoirs (e.g., sandstones, carbonates, and mudrocks) – pore shape, pore-size distribution, and pore connectivity – control fluid flow and hydrocarbon movement
- Effective porosity is the portion of connected pore space as conductive pathways to participate in flow and movement
- This work discusses various approaches to quantifying effective porosity for a range of oil and gas reservoirs

Definition and Problem Statement

Porosity of Geological Media

$$n(\phi)=\frac{V_v}{V_t}=\frac{V_t-V_s}{V_t}$$ (1350-1400)

$$n=1-\frac{\rho_b}{\rho_p}$$

$$Q=-KA\frac{dh}{dL}$$ Darcy (1856)

Slichter (1899)

Meinzer (1923)

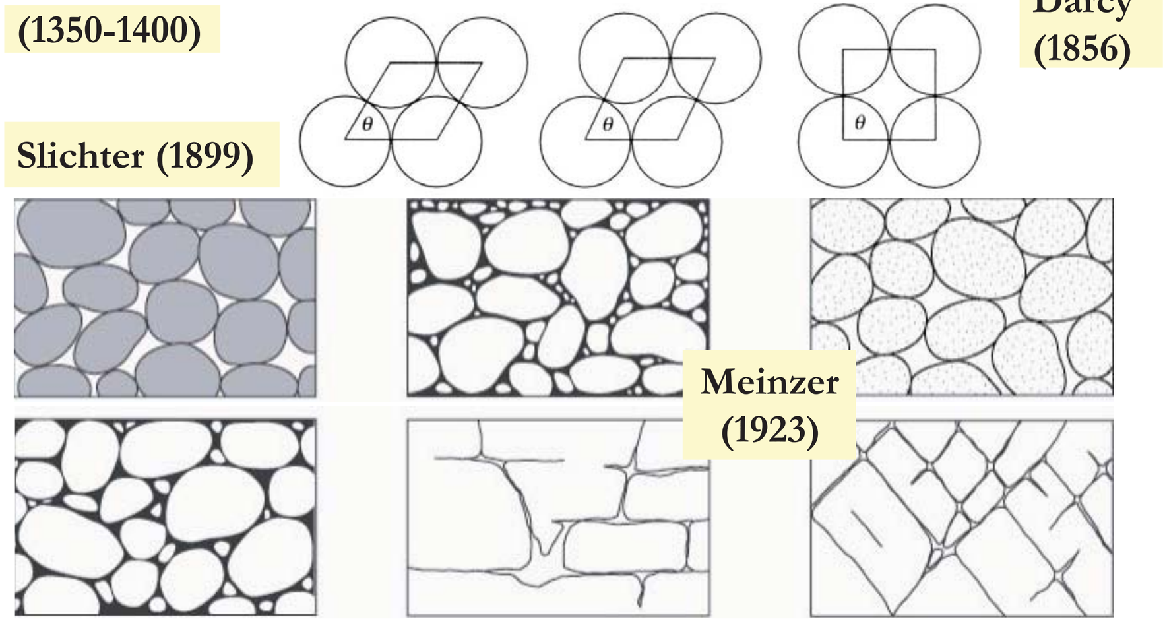

Measuring ϕ

Gas pycnometry (universal gas law)

Mass lost upon drying a saturated sample

Either of the above, both before and after pulverizing (but to what size?)

$$\phi=1-\frac{\rho_b}{\rho_p}$$ (assuming uniform mineralogy)

2D "porosity" of a thin section (DeLesse's theorem, 1848; a fraction of area is equal to fractions of volume in infinitely thin section)

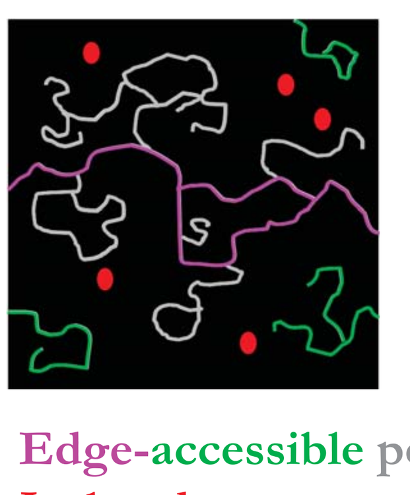

Edge-accessible pores

Isolated pores

X-ray microtomography & reconstruction

Range of Porosity and Practical Cutoff

What is good porosity

- 0–5%—Negligible
- 5–10%—Poor
- 10–15%—Fair
- 15–20%—Good
- >20%Very good
- Practical cutoff for oil sandstone ~8%
- Cut off for limestone ~5%
- For gas reservoirs, the cutoff is lower

Conventional classifications

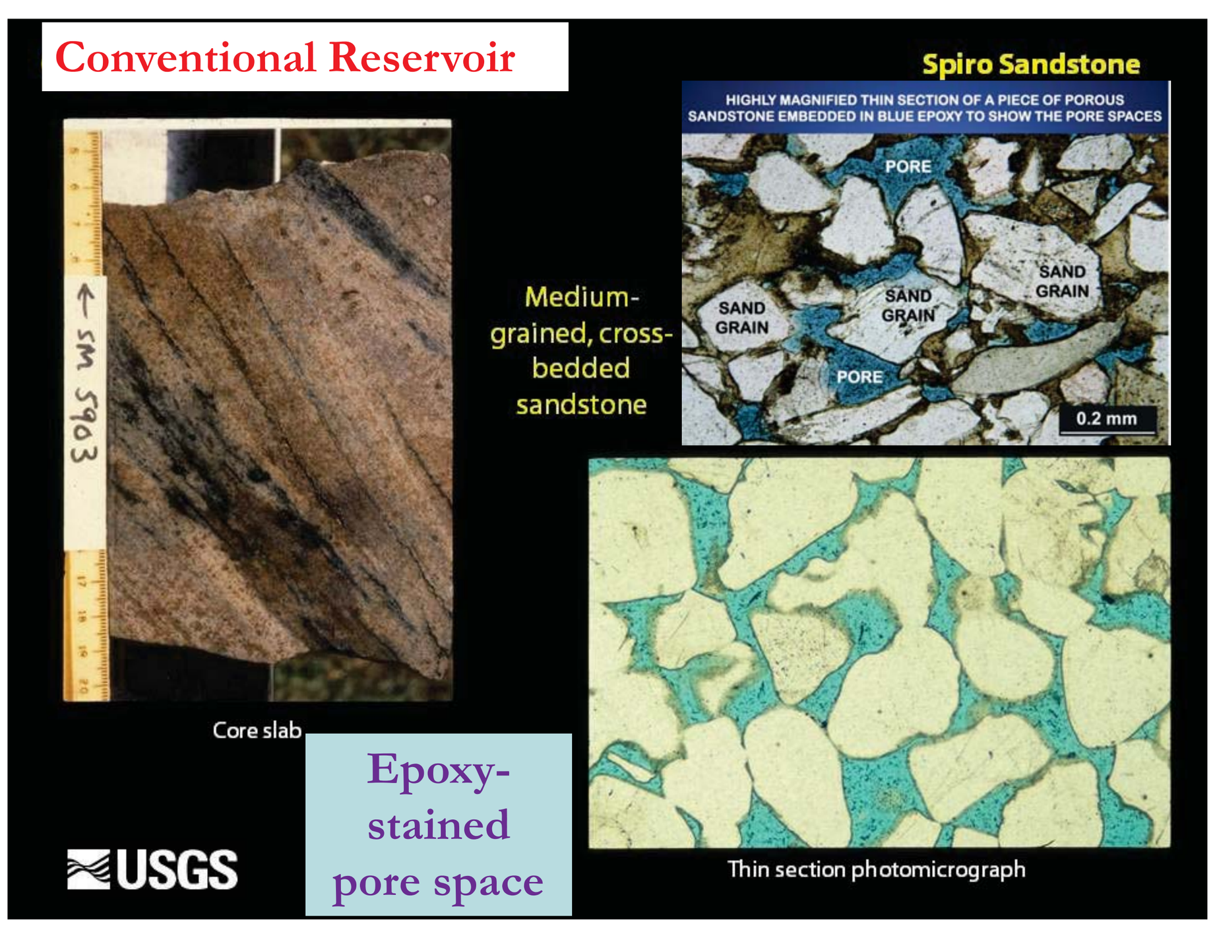

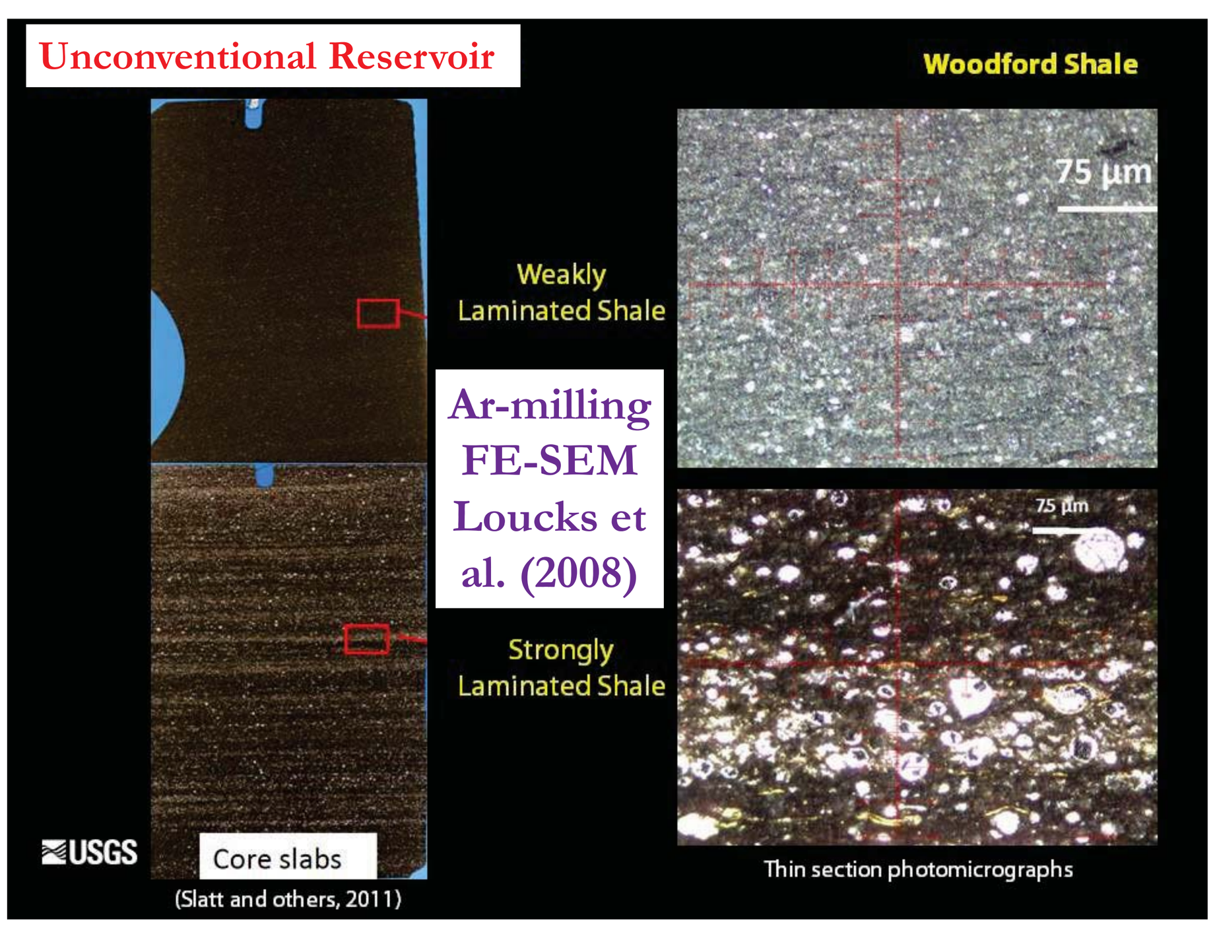

Total ϕ_τ vs. Effective Porosity ϕ_e

- Total porosity: include isolated pores, dead-end pores, adhesive liquid, or any other liquid that does not actively move, as well as trapped gas
- Effective: ratio between the inter-connected pore void volume and the total volume of the rock

Porosity available for fluid flow and mass transport

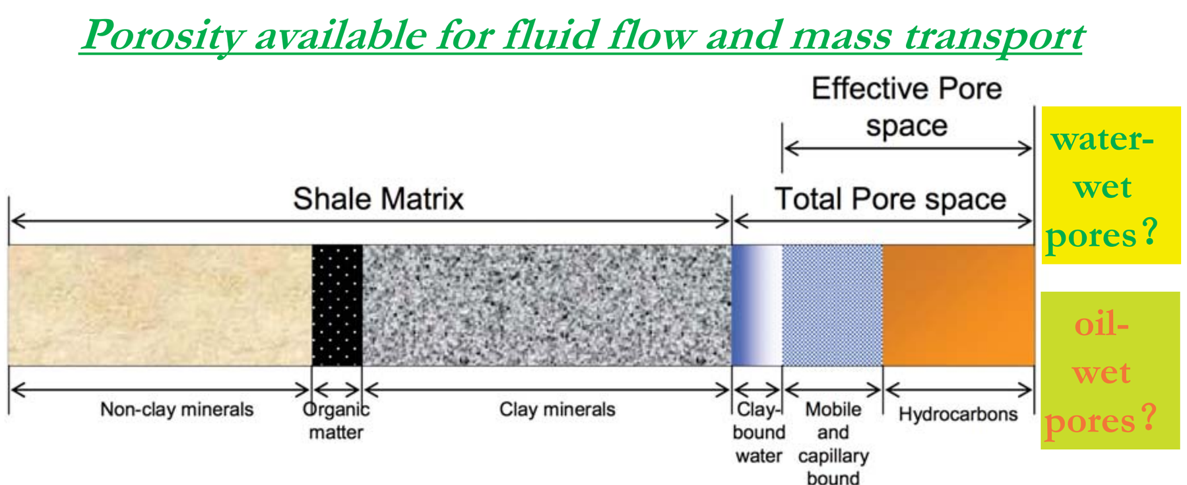

Pore Structure: Geometry and Topology

Percolation theory: the mathematics of how macroscopic properties emerge from local (microscopic) connections

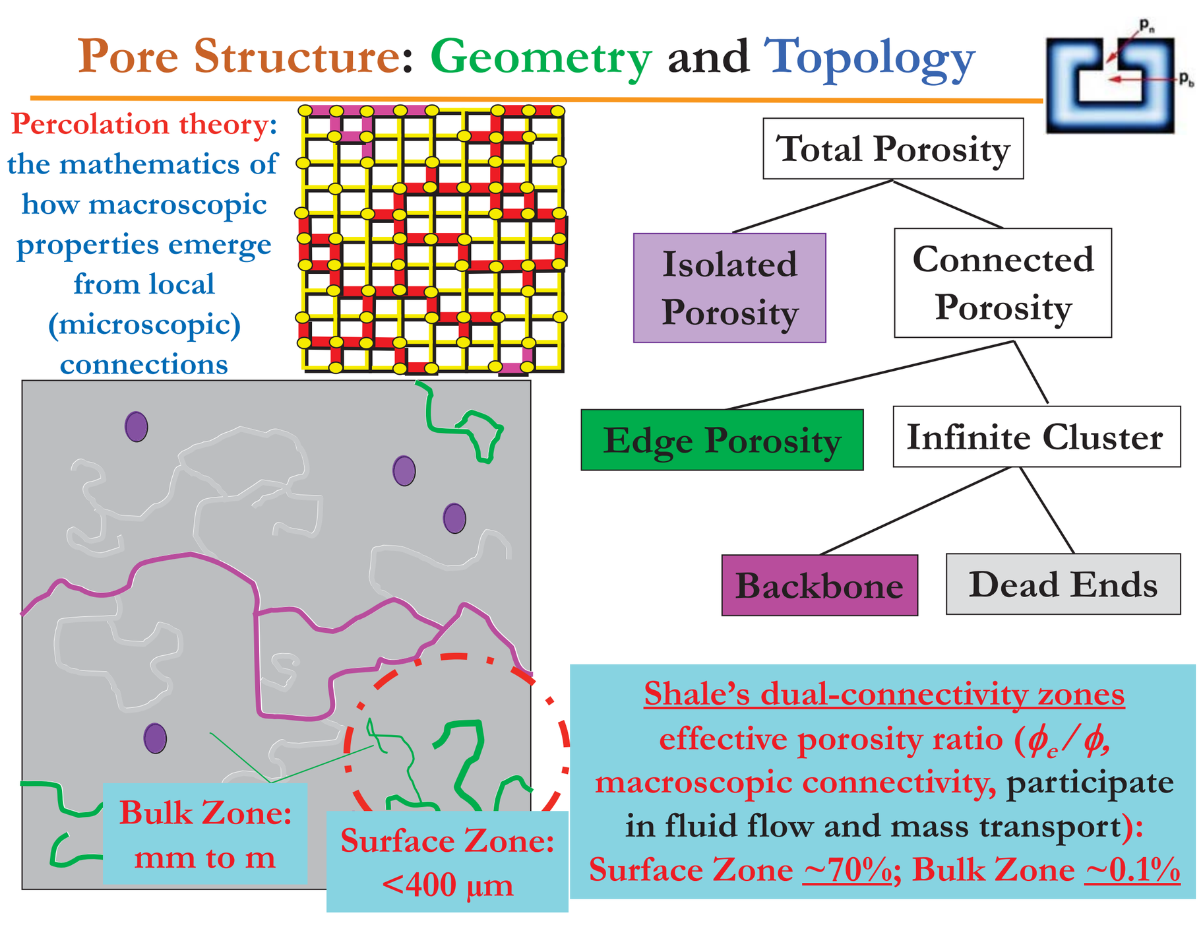

Shale's dual-connectivity zones effective porosity ratio (ϕ_e/ϕ_t), macroscopic connectivity, participate in fluid flow and mass transport): Surface Zone ~70%; Bulk Zone ~0.1%

Range in values of total porosity

Material	Total Porosity (%)	Effective Porosity (%)
Anhydrite[a]	0.5–5	0.05–0.5
Chalk[a]	5–40	0.05–2
Limestone, dolomite[a]	0–40	0.1–5
Sandstone[a]	5–15	0.5–10
Shale[a]	1–10	0.5–5
Salt[a]	0.5	0.1
Granite[b]	0.1	0.0005
Fractured crystalline rock[b]	—	0.00005 – 0.01

[a] Data from Croff et al. (1985).
[b] Data from Norton and Knapp (1977).

Norton, D., and R. Knapp. 1977. Transport phenomena in hydrothermal systems: Nature of porosity. *Am. J. Sci.*, 27: 913–936.

Edge-accessible Effective Porosity

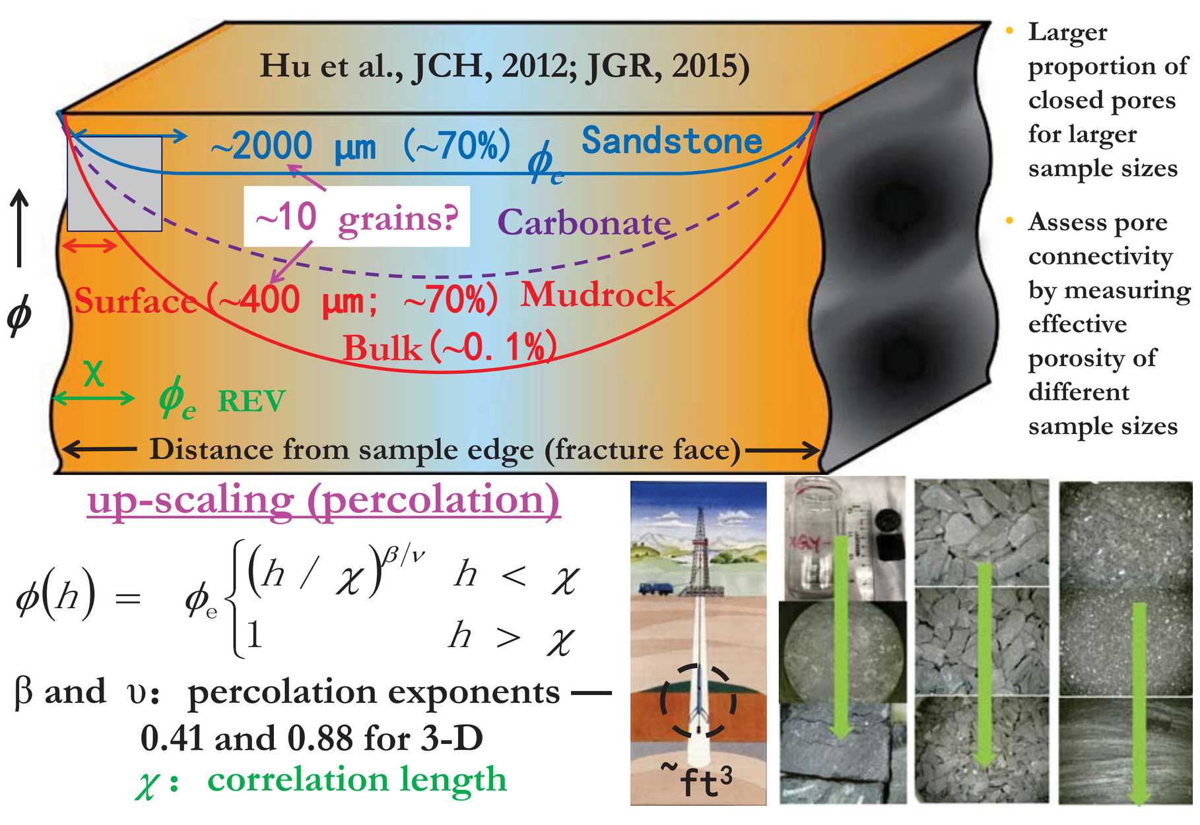

- Larger proportion of closed pores for larger sample sizes
- Assess pore connectivity by measuring effective porosity of different sample sizes

$$\phi(h)=\phi_c\begin{cases}(h/\chi)^{\beta/\nu} & h<\chi\\ 1 & h>\chi\end{cases}$$

β and ν: percolation exponents — 0.41 and 0.88 for 3-D

χ: correlation length

Approach: Vacuum Saturation

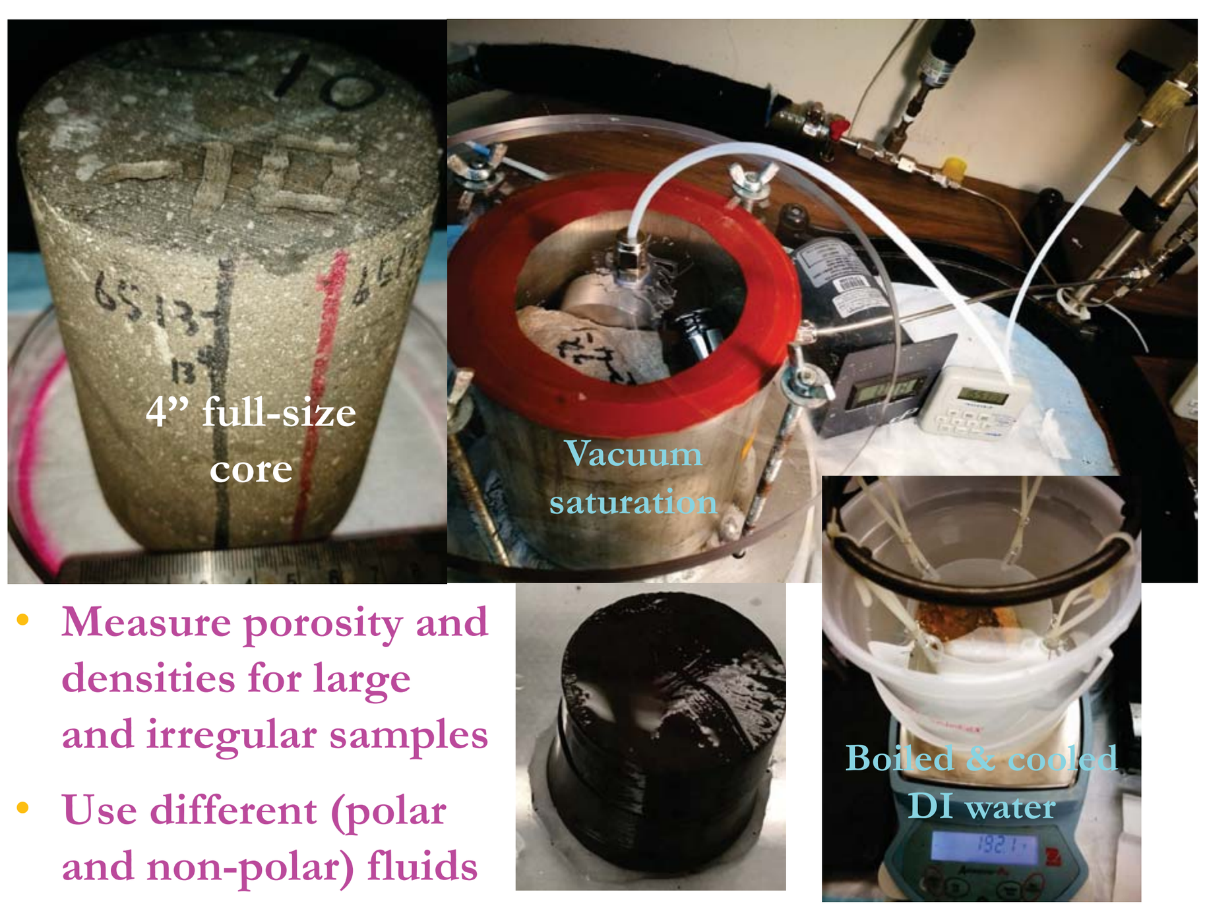

- Measure porosity and densities for large and irregular samples
- Use different (polar and non-polar) fluids

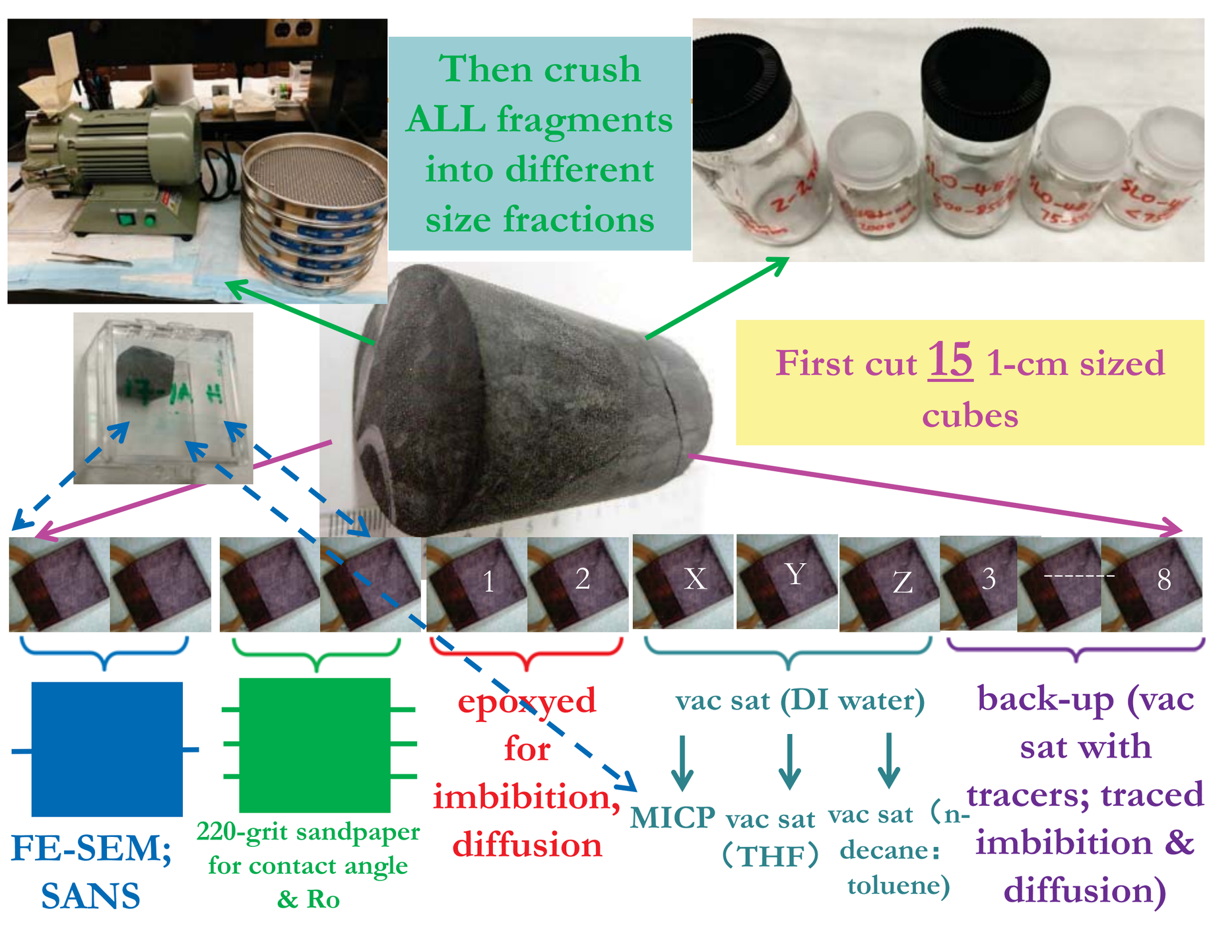
Then crush ALL fragments into different size fractions
First cut 15 1-cm sized cubes
FE-SEM; SANS
220-grit sandpaper for contact angle & Ro
epoxied for imbibition, diffusion
MICP
vac sat (DI water)
vac sat (THF)
vac sat (n-decane; toluene)
back-up (vac sat with tracers; traced imbibition & diffusion)

Approach: Mercury Intrusion Capillary Pressure

Accessibility, Permeability, and Tortuosity: MICP

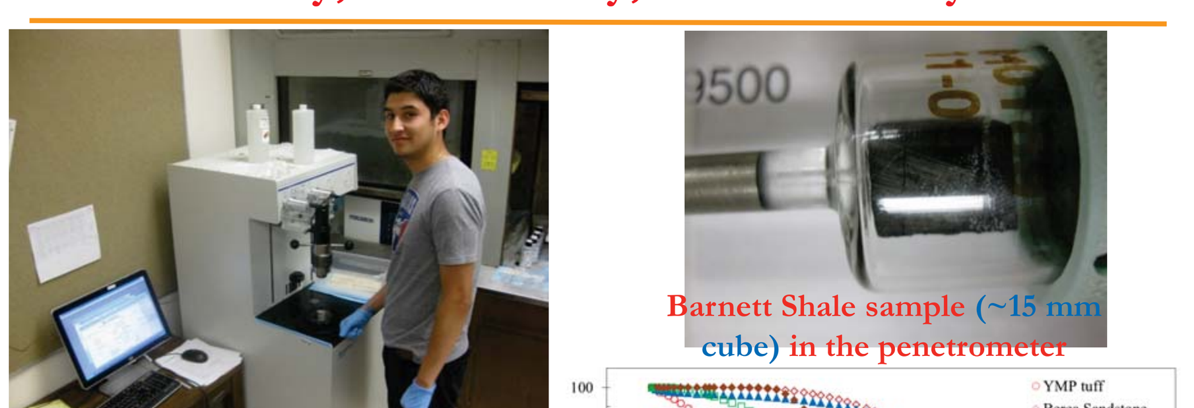

- Mercury Injection Capillary Pressure (MICP)
- Measurable pore-throat diameter range: 2.8 nm to 500 μm
- A mercury atom is about 0.3 nm in diameter

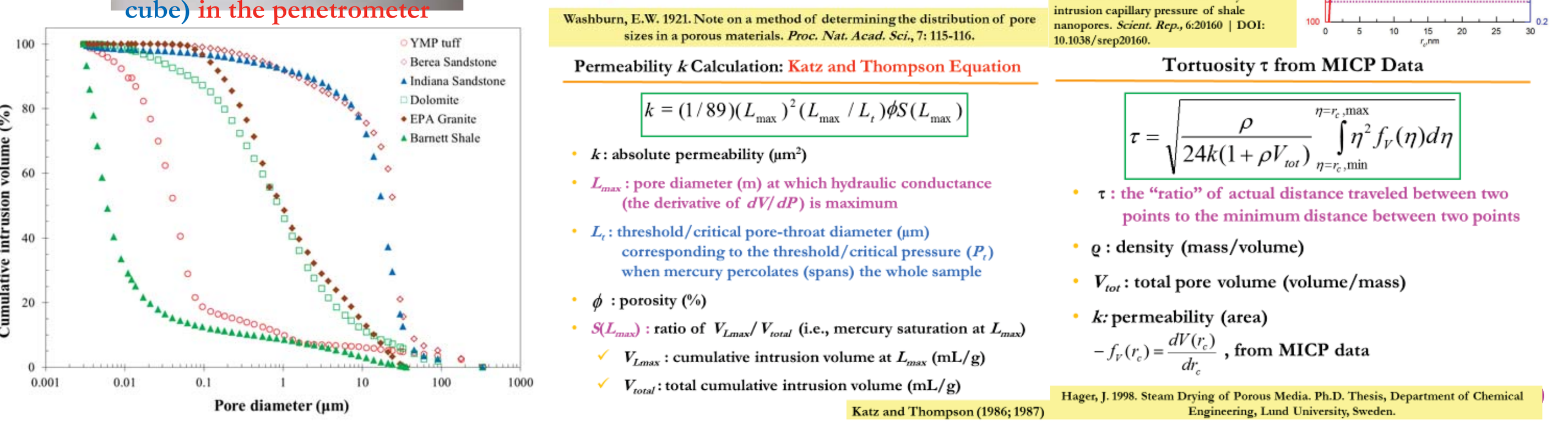
Washburn Equation
D: equivalent pore-throat diameter (μm)
W: Washburn unit conversion factor (0.145)
γ: interfacial tension (485 dynes/cm for Hg)
θ: contact angle (130-140° for Hg in most solids)
P: capillary pressure between mercury and air (psia)
Permeability & Calculation: Katz and Thompson Equation
k: absolute permeability
ϕ: porosity (%)
Tortuosity τ from MICP Data
τ: the "ratio" of actual distance traveled between two points to the minimum distance between two points
ρ: density (mass/volume)
Vtot: total pore volume (volume/mass)
k: permeability (area)

MICP Analysis: Blank Correction, Validity, and Detection Limit

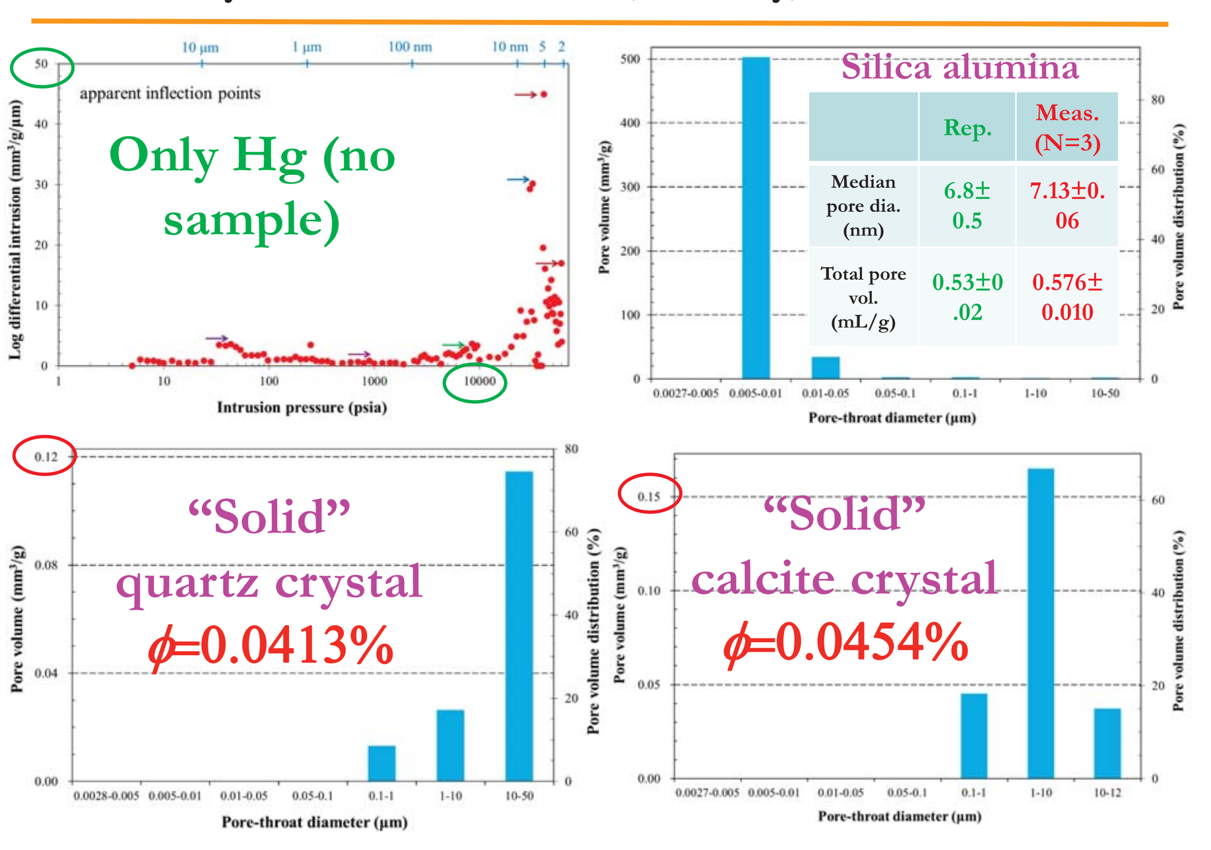

MICP Analysis: Pore-Size Distributions vs. Grain Sizes

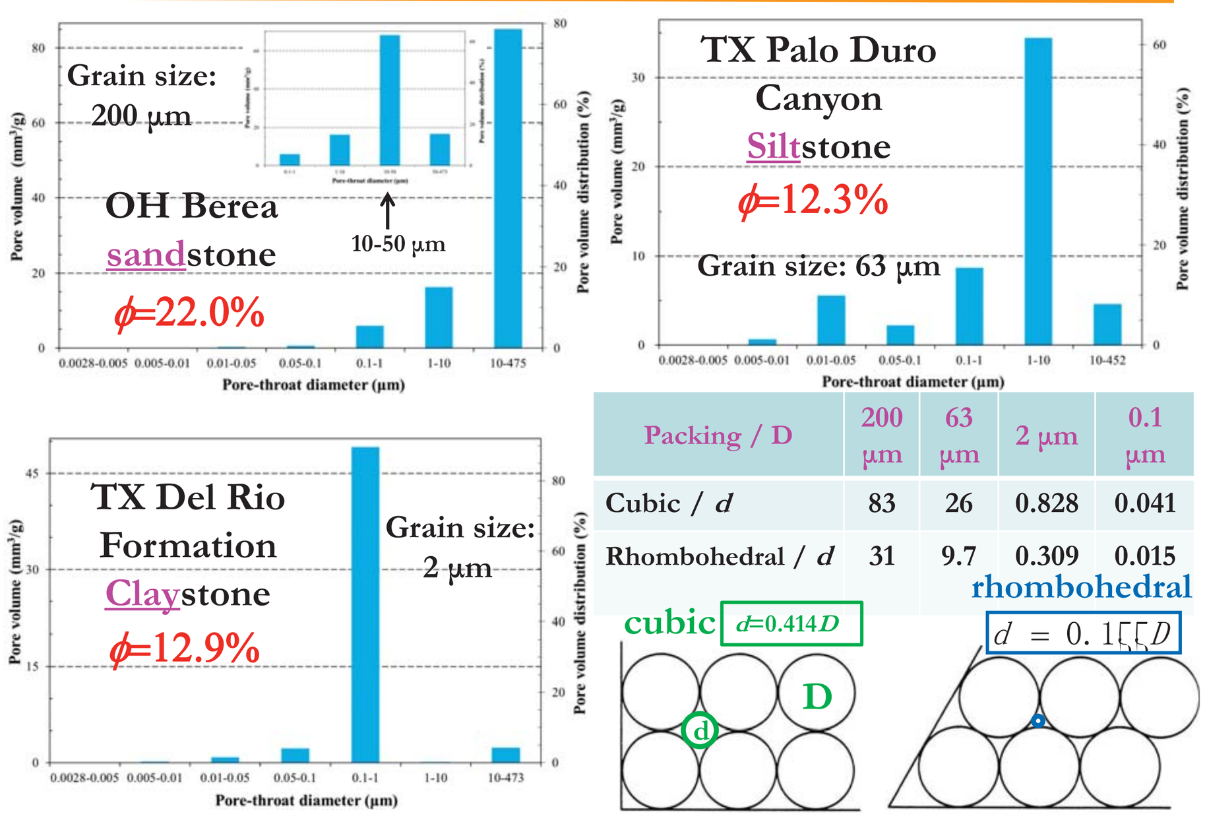

Packing / D	200 μm	63 μm	2 μm	0.1 μm
Cubic / *d*	83	26	0.828	0.041
Rhombohedral / *d*	31	9.7	0.309	0.015

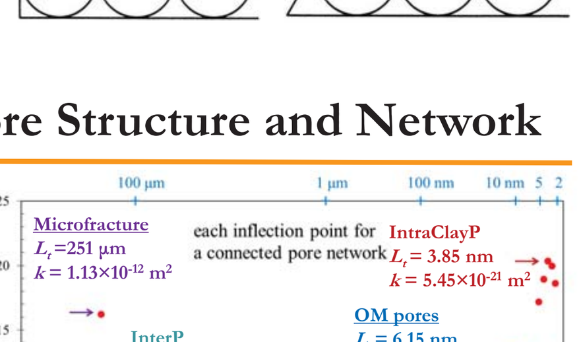

Global Benchmarking Tests: KG²B Project (2015-2017)

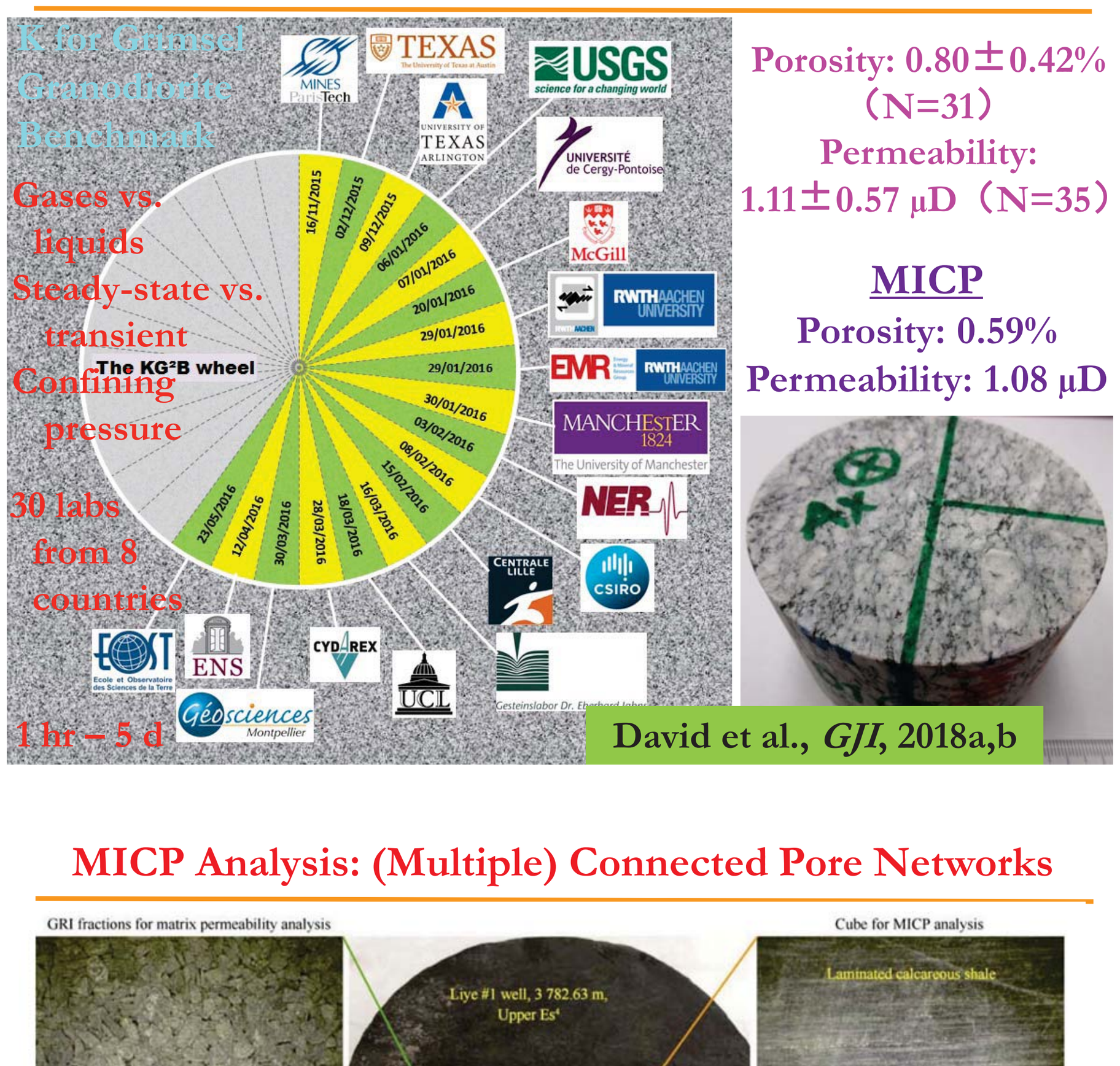

Porosity: 0.80 ± 0.42% (N=31)

Permeability: 1.11 ± 0.57 μD (N=35)

MICP

Porosity: 0.59%

Permeability: 1.08 μD

David et al., *GJI*, 2018a,b

MICP Analysis: (Multiple) Connected Pore Networks

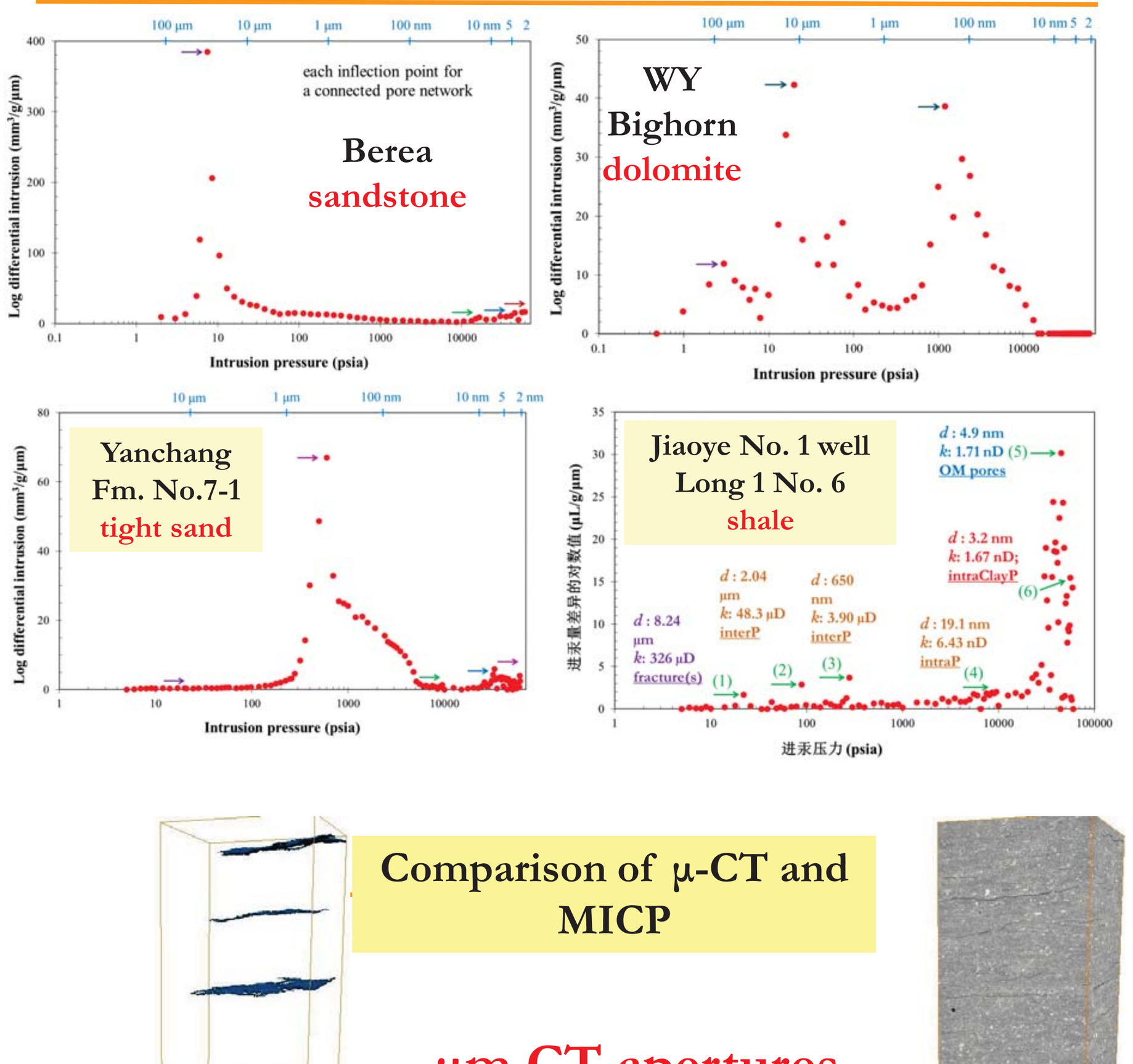

MICP Analysis: Shale Pore Structure and Network

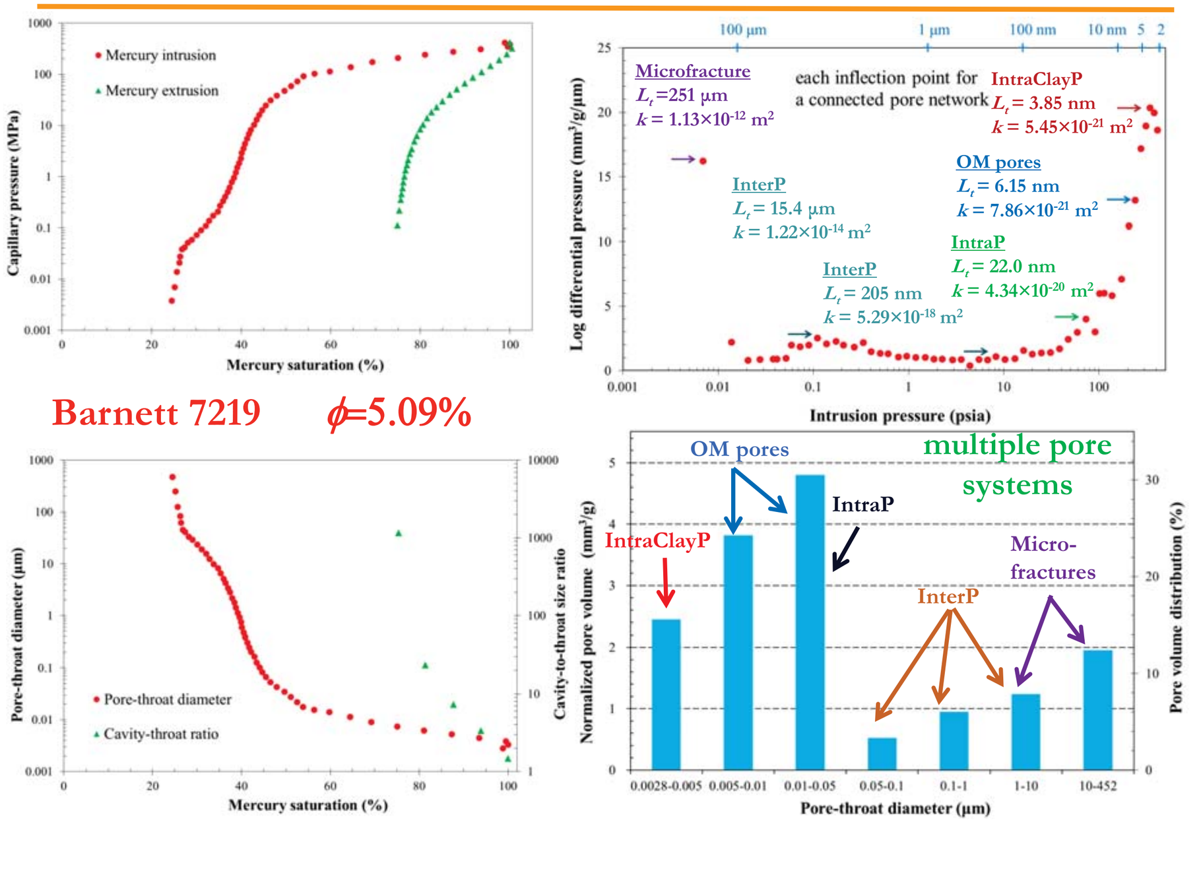
Barnett 7219 ϕ=5.09%
Microfracture Lt=251 μm k = 1.13×10-12 m2
each inflection point for a connected pore network
IntraClayP Lt = 3.85 nm k = 5.45×10-21 m2
OM pores Lt = 6.15 nm k = 7.86×10-21 m2
InterP Lt = 15.4 μm k = 1.22×10-14 m2
InterP Lt = 205 nm k = 5.29×10-18 m2
IntraP Lt = 22.0 nm k = 4.34×10-20 m2
OM pores
multiple pore systems
IntraClayP
IntraP
InterP
Micro-fractures
Pore-throat diameter
Cavity-throat ratio
Mercury saturation (%)
Pore-throat diameter (μm)

MICP Analysis: (Multiple) Connected Pore Networks

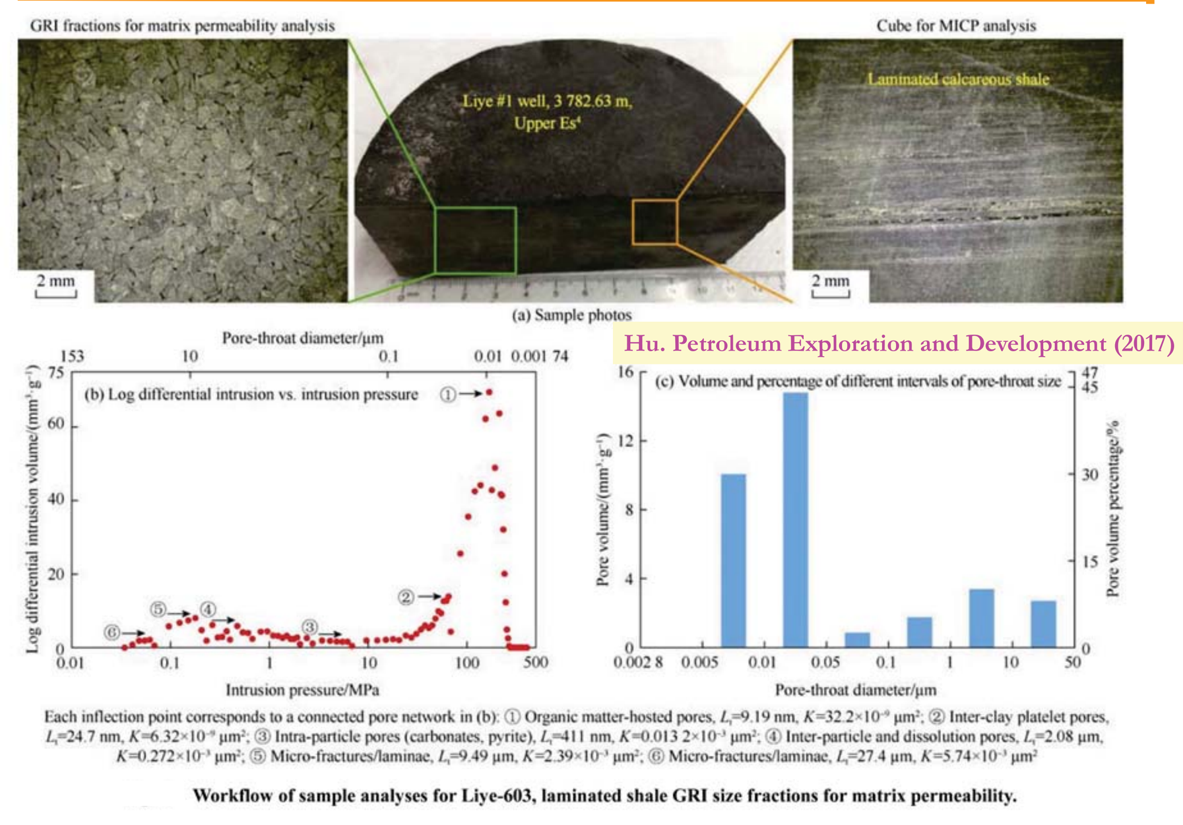

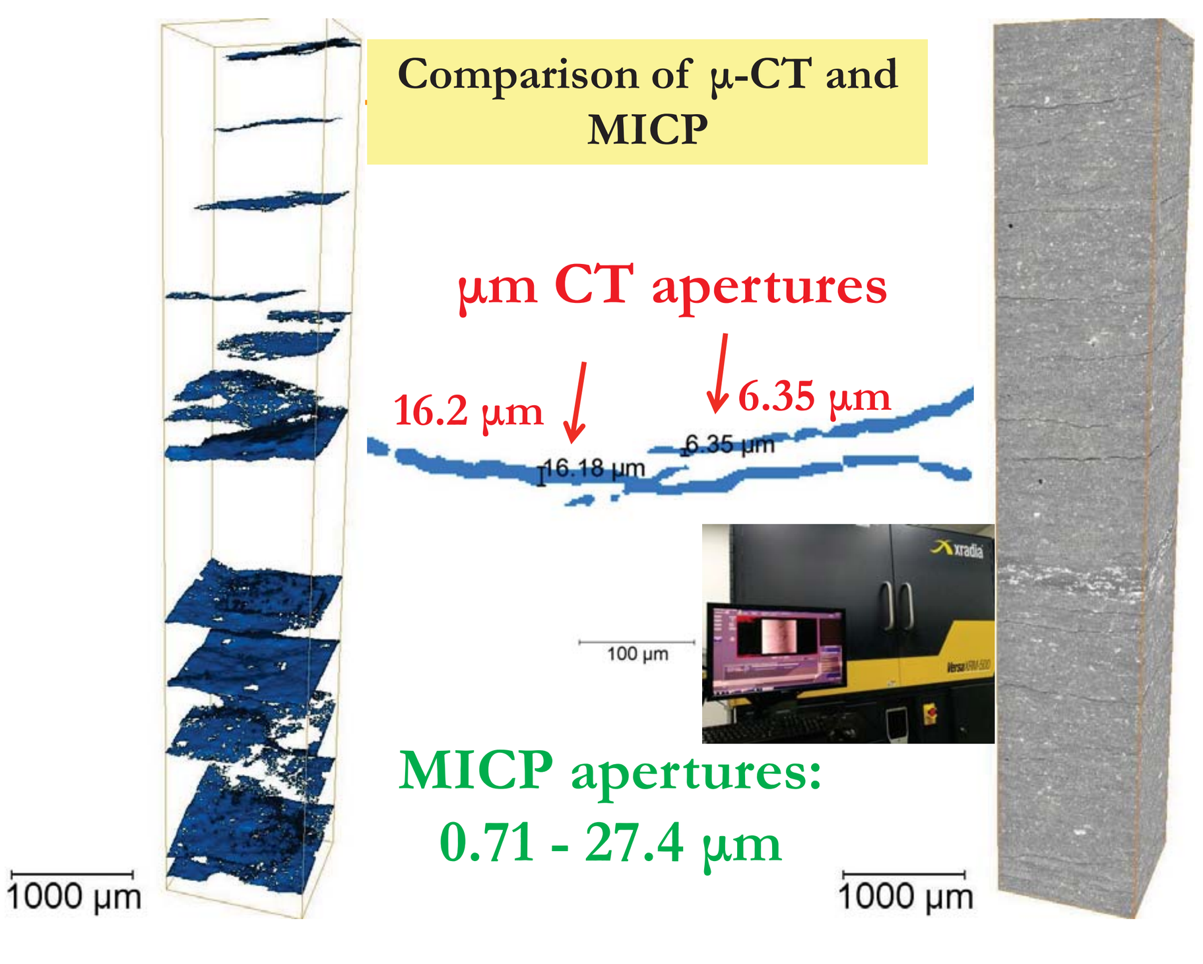

A Range of Sample Sizes: Effective Porosity and Different Exp.

Size designation	Sieve mesh	Size fraction (diameter)	Equivalent spherical dia. (μm)	Equivalent spherical dia. (mm)
Cylinder / Plug		2.54 cm dia.; any height (*e.g., 3 cm*)	(24394)	(24.39)
Cube		1.0 cm	9086	9.086
GRI+	#8 to #12	1.70 - 2.36 mm	2030	2.030
Size A	#12 to #20	841 - 1700 μm	1271	1.271
GRI	#20 to #35	500 - 841 μm	671	0.671
Size B	#35 to #80	177 - 500 μm	339	0.339
Size C	#80 to #200	75 - 177 μm	126	0.126
Powder	<#200	< 75 μm	< 75	< 0.075
Size D	#200 to #625	20 - 75 μm	47.5	0.0475
Size E	<635	<20 μm	<20	<0.02

Overlaps Surface Zone and Bulk Zone

TX Wolfcamp Sample of Different Sizes: Inter- vs. Intra-granular Pores

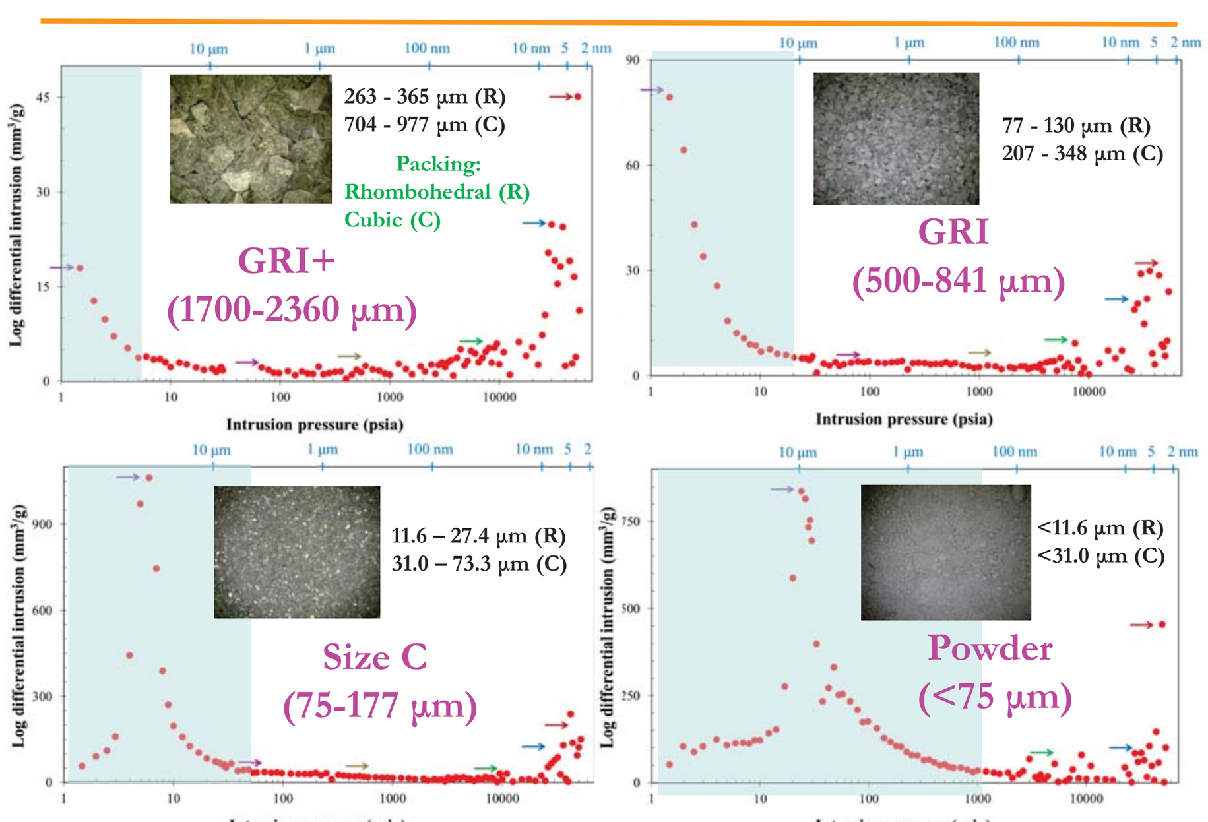

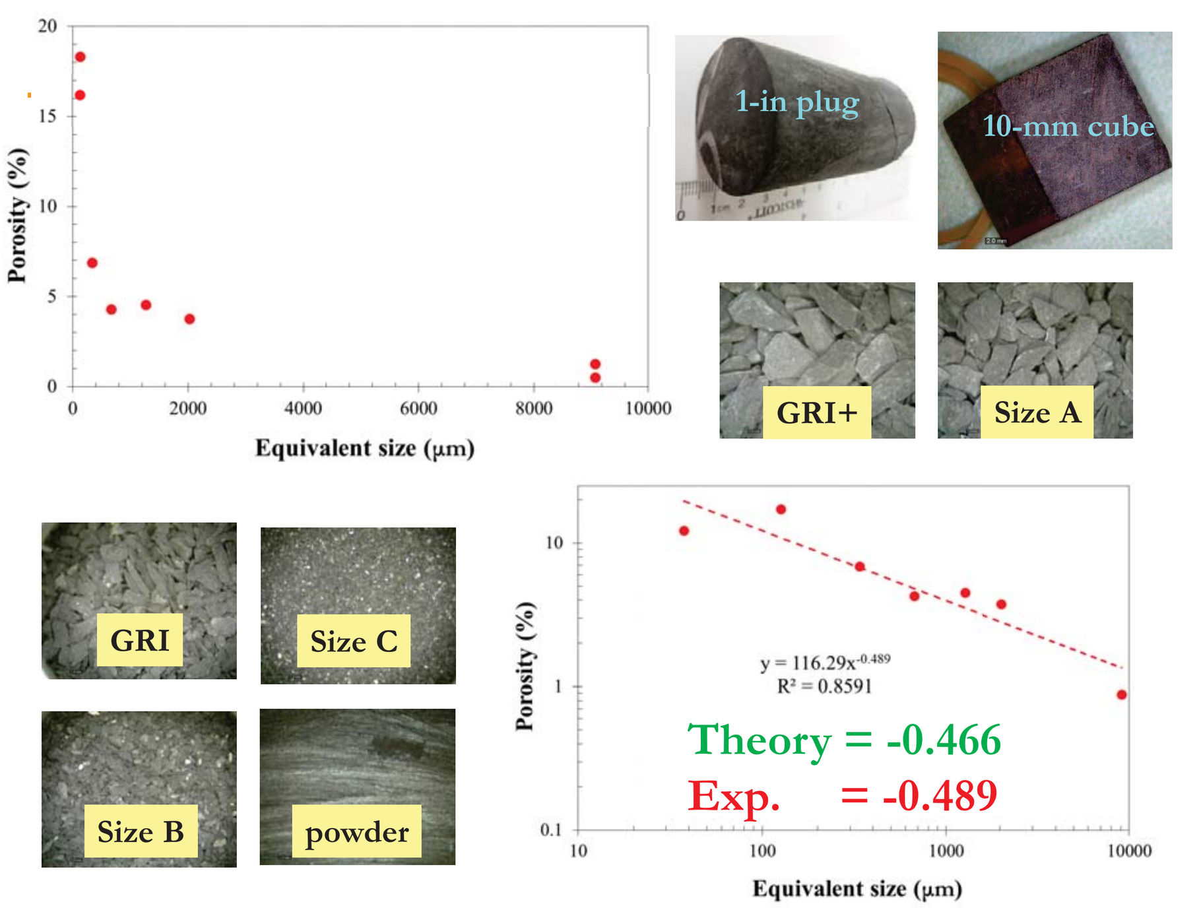

Approach: Wood's Metal Impregnation and Imaging

Wood's Metal Intrusion and Imaging

- A quaternary alloy of Bi (50%), Cd (12.5%), Pb (25%), and Sn (12.5%), with a slightly different proportion
- A corresponding melting point 65 to 80°C
- Used in natural rock, cement paste, concrete, coal; started at UC Berkeley in late 1970s Swanson, JPT, 1979

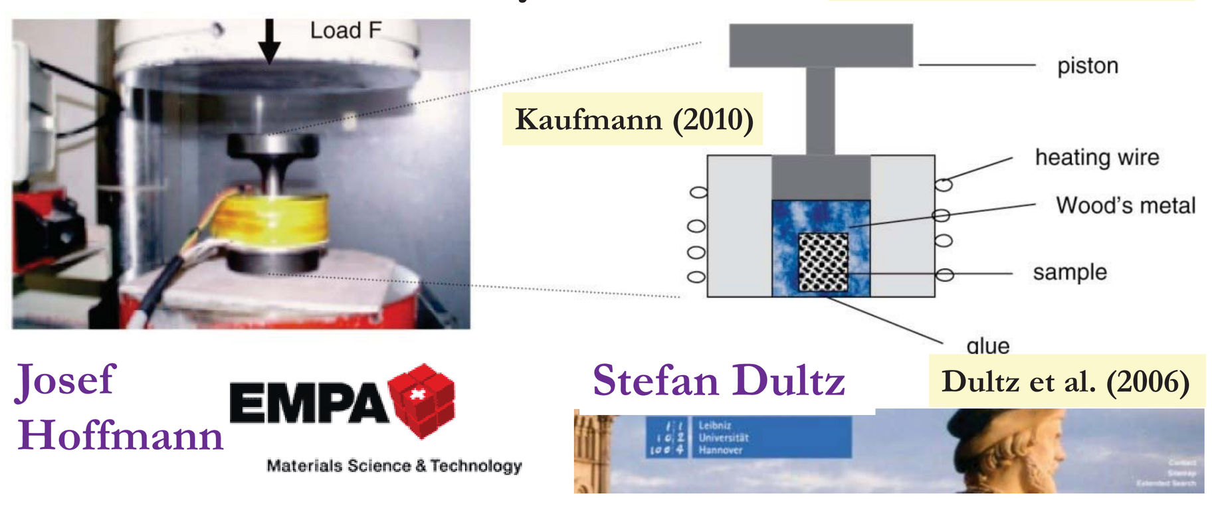

Porosity

- Image (500 μm × 500 μm): 23.7%
- MICP (1 cm × 1 cm × 1 cm): 21.0±0.147%

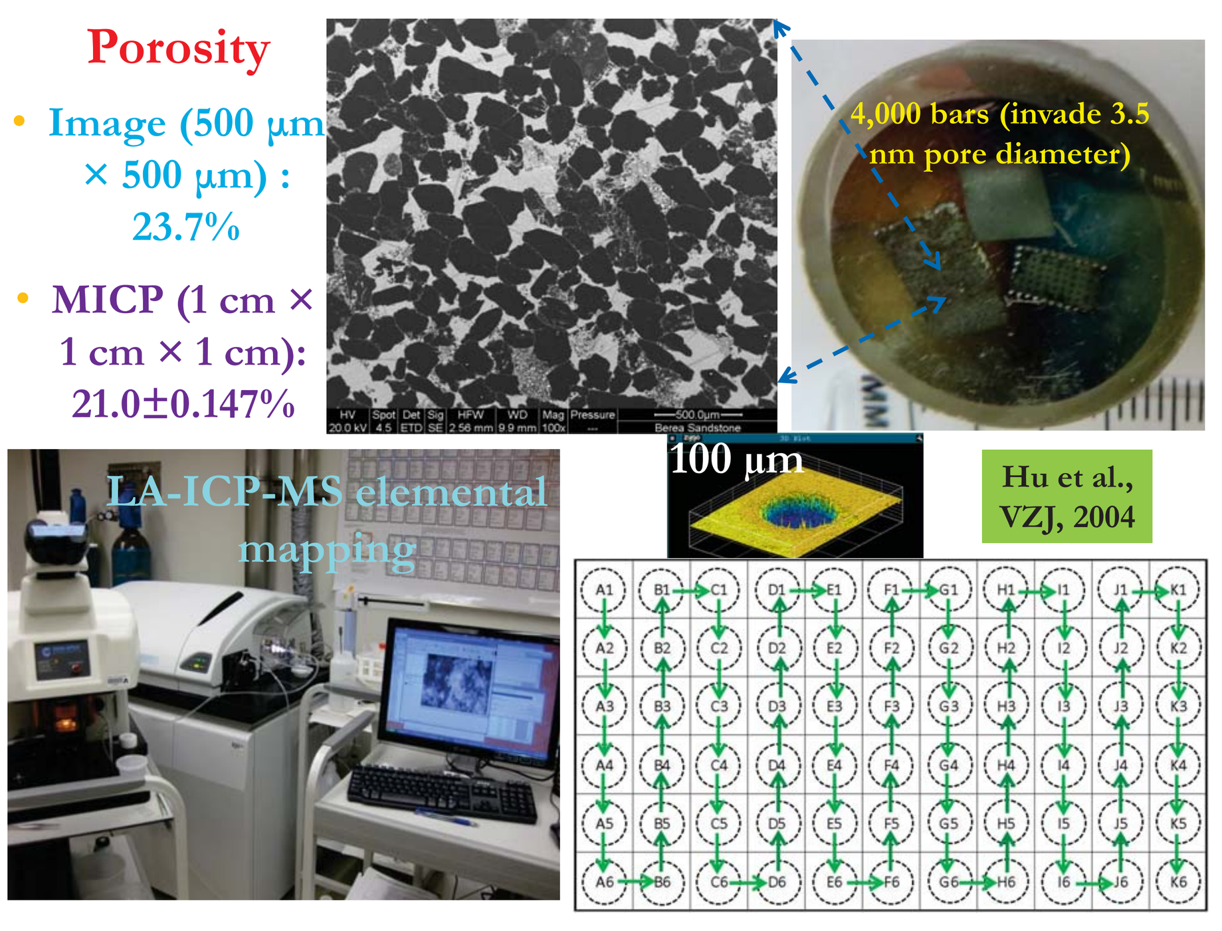

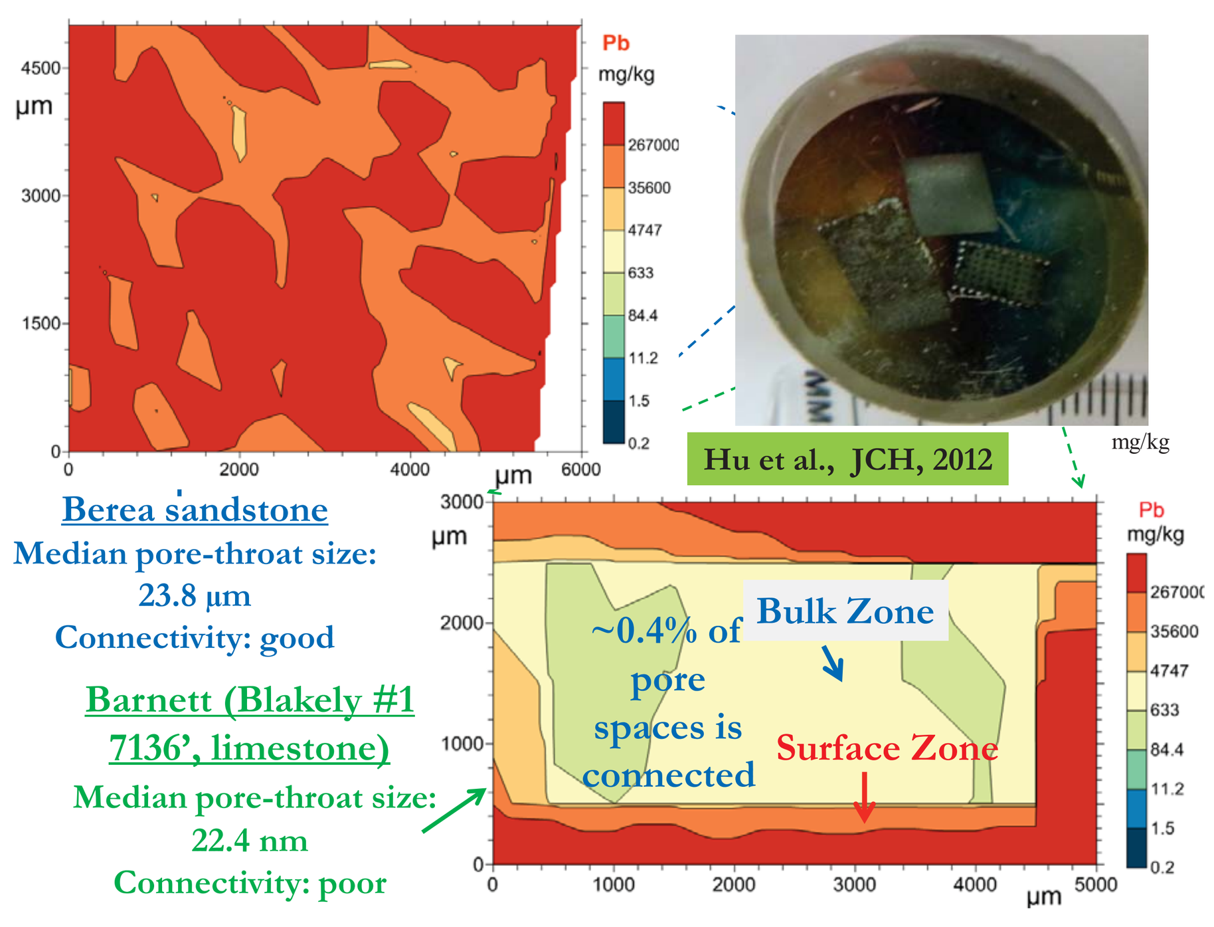

Approach: Fluid Imbibition and Tracer Migration

Mixed Wettability and Associated Pore Structure

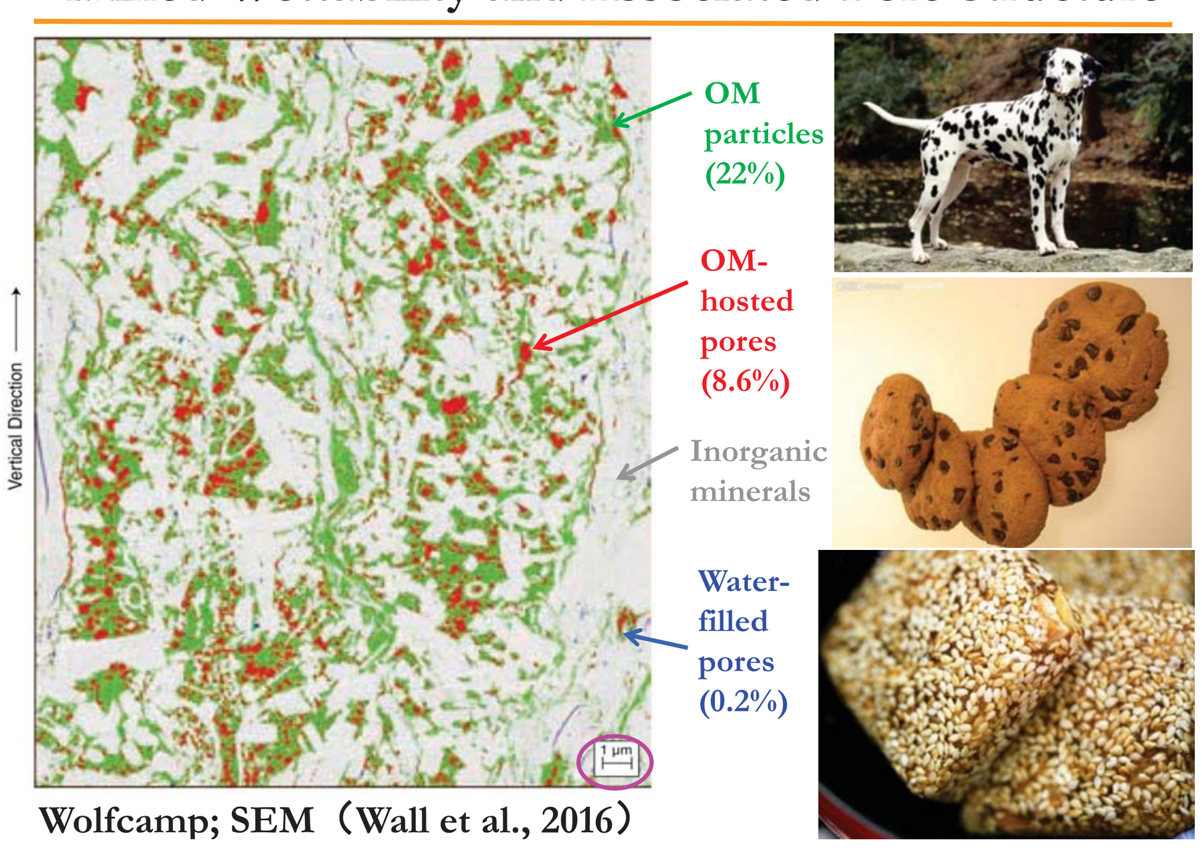

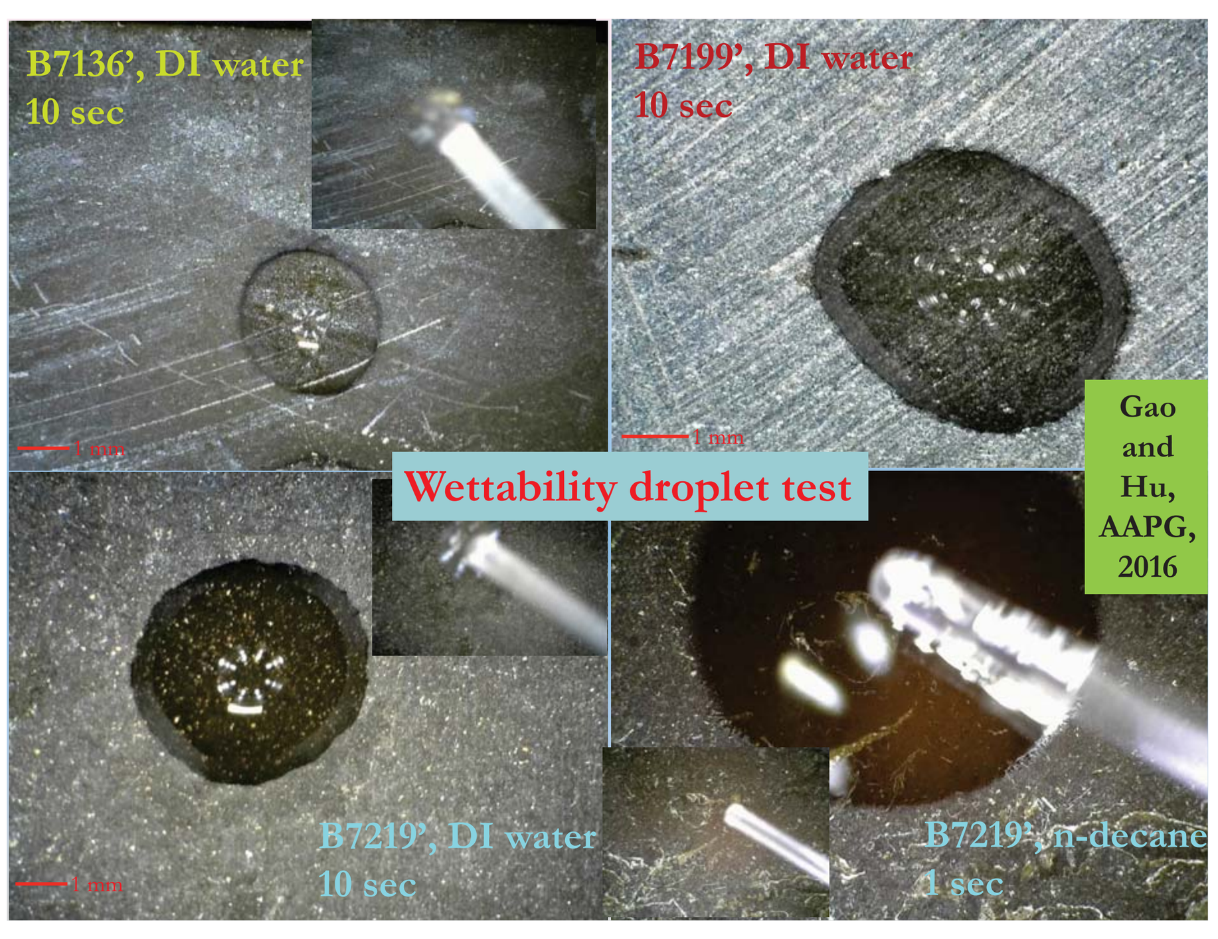

Contact Angle Measurements with Different Fluids

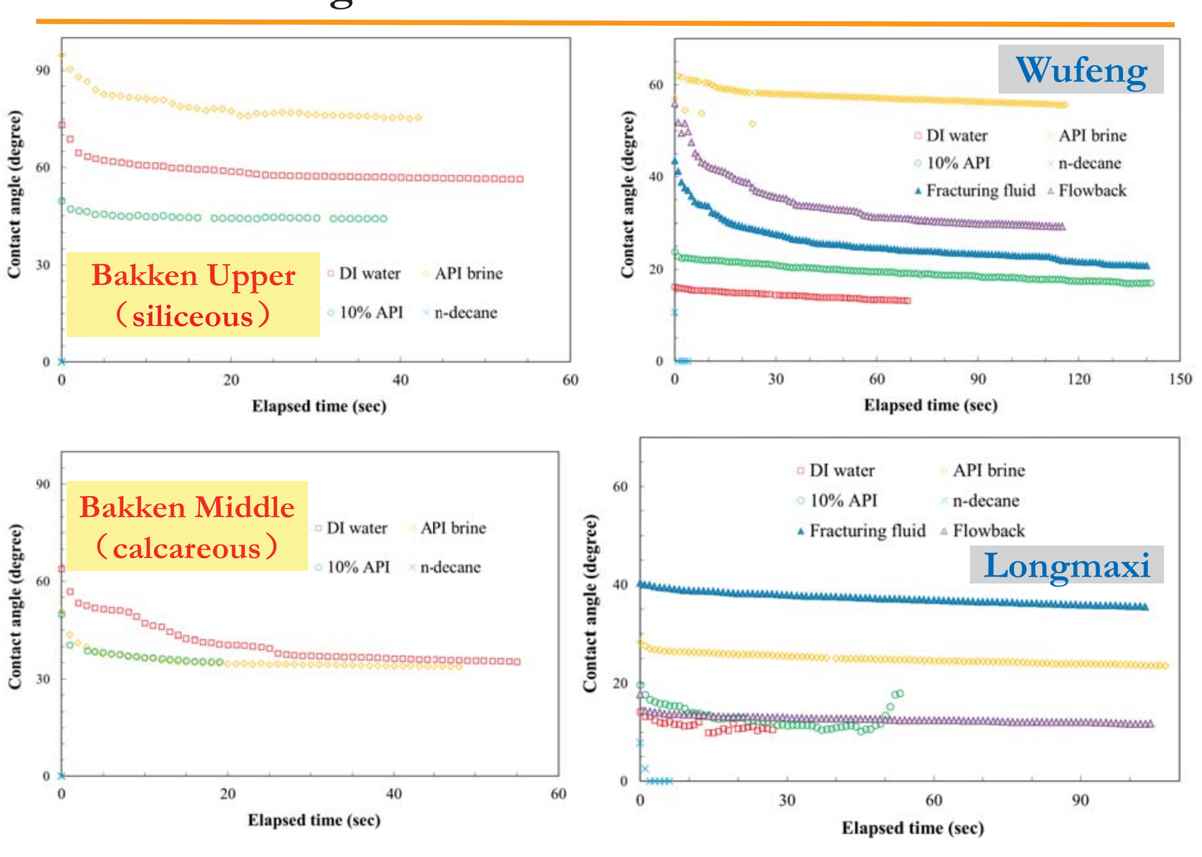

Wettability: Phase-based Fluids and Tracers

- API brine – water (0.394 nm) wetting
  - ReO_4^- (0.553 nm), I^- (0.220 nm); non-sorbing
  - Cs^+, Co^{2+}, Sm^{3+} (0.13 nm; sorbing)
  - Anionic Sb-complex (0.89 nm)
  - Cationic Ru-complex (1.0 nm)
  - CdS nanoparticles (5–10 nm)
- n-decane (1.535 nm) – oil wetting
  - organic-I
  - organic-Re
  - CdTe nanoparticles (5–8 nm)

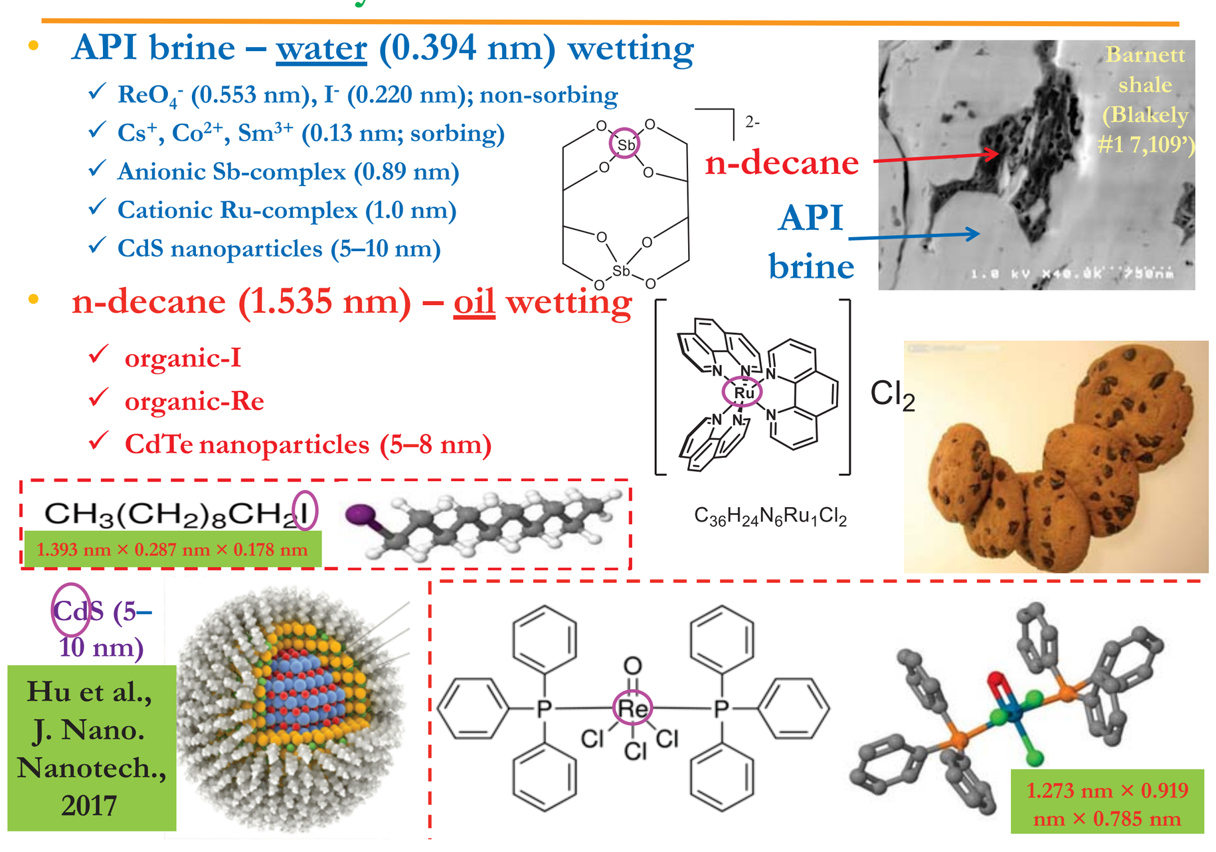

2D/3D Mapping Scheme by LA-ICP-MS

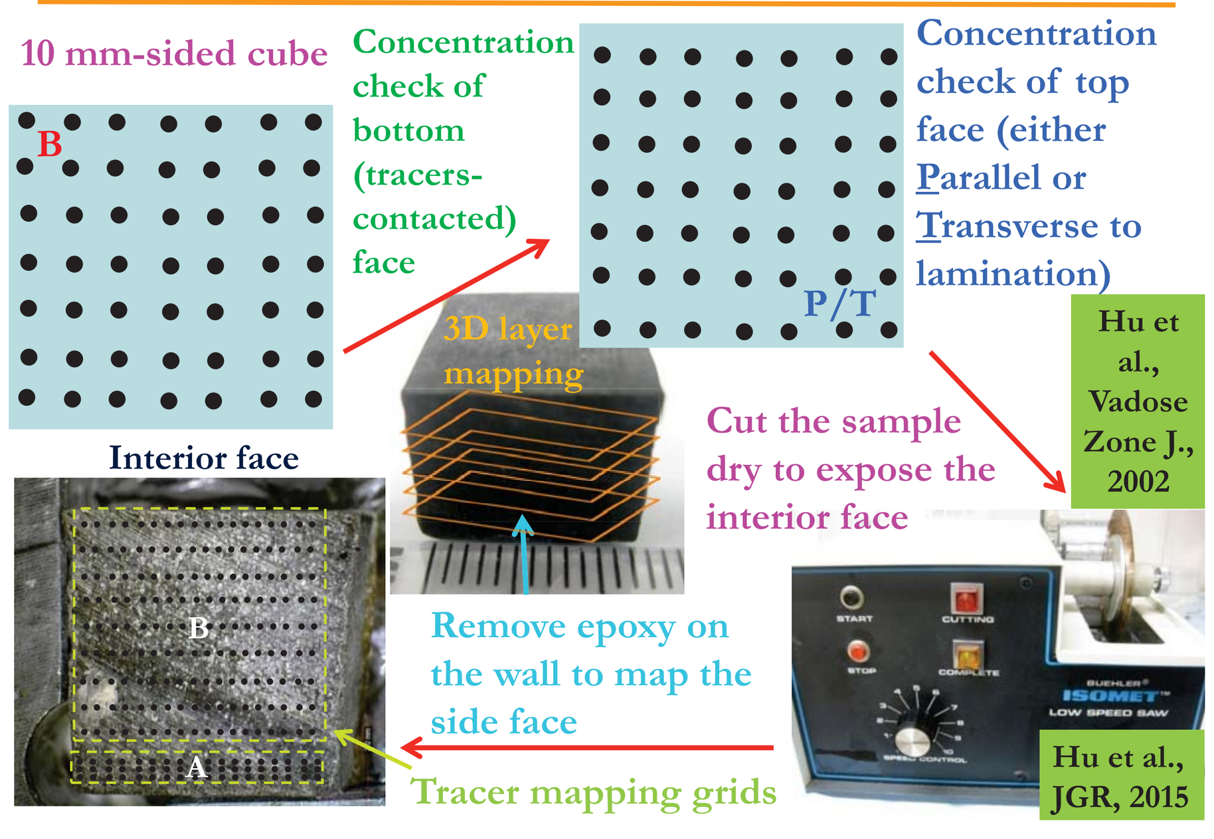

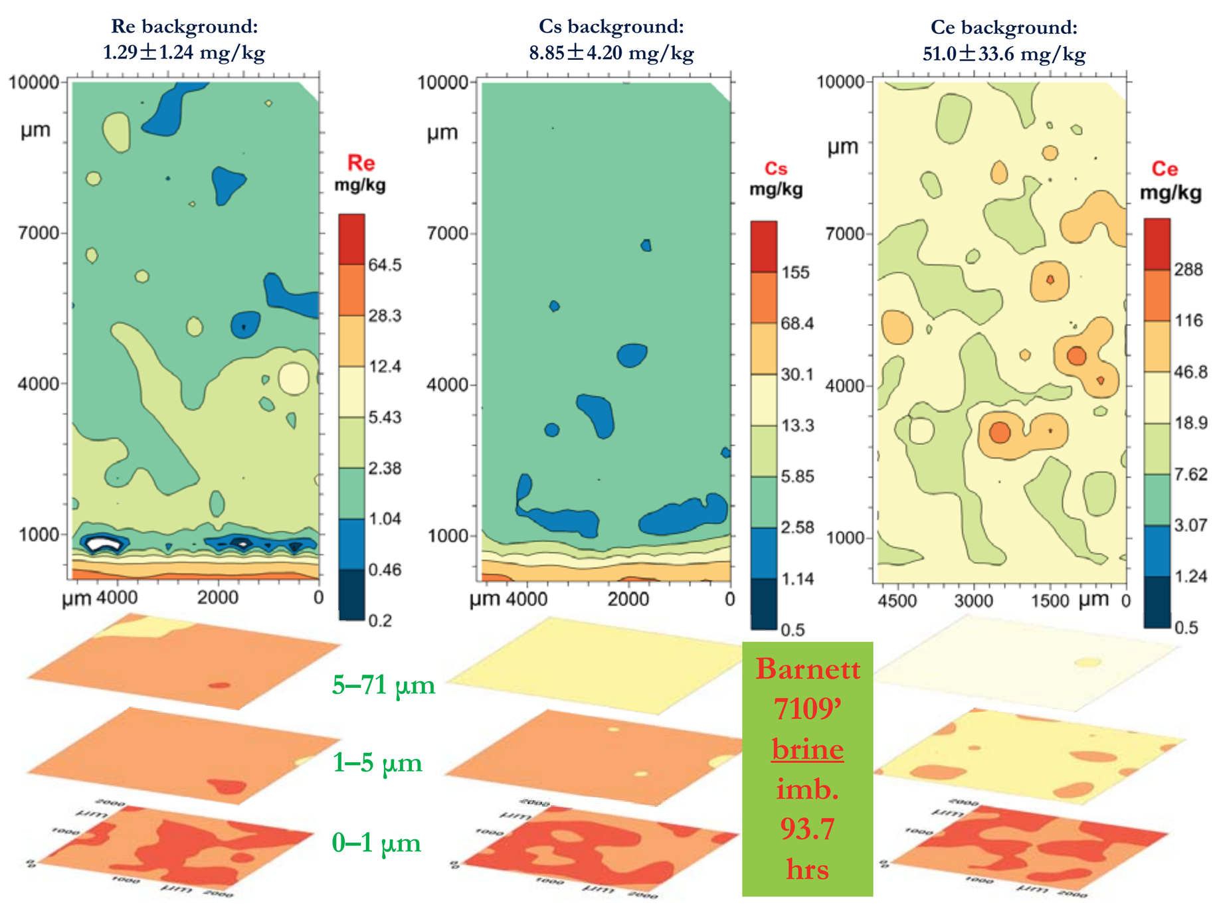

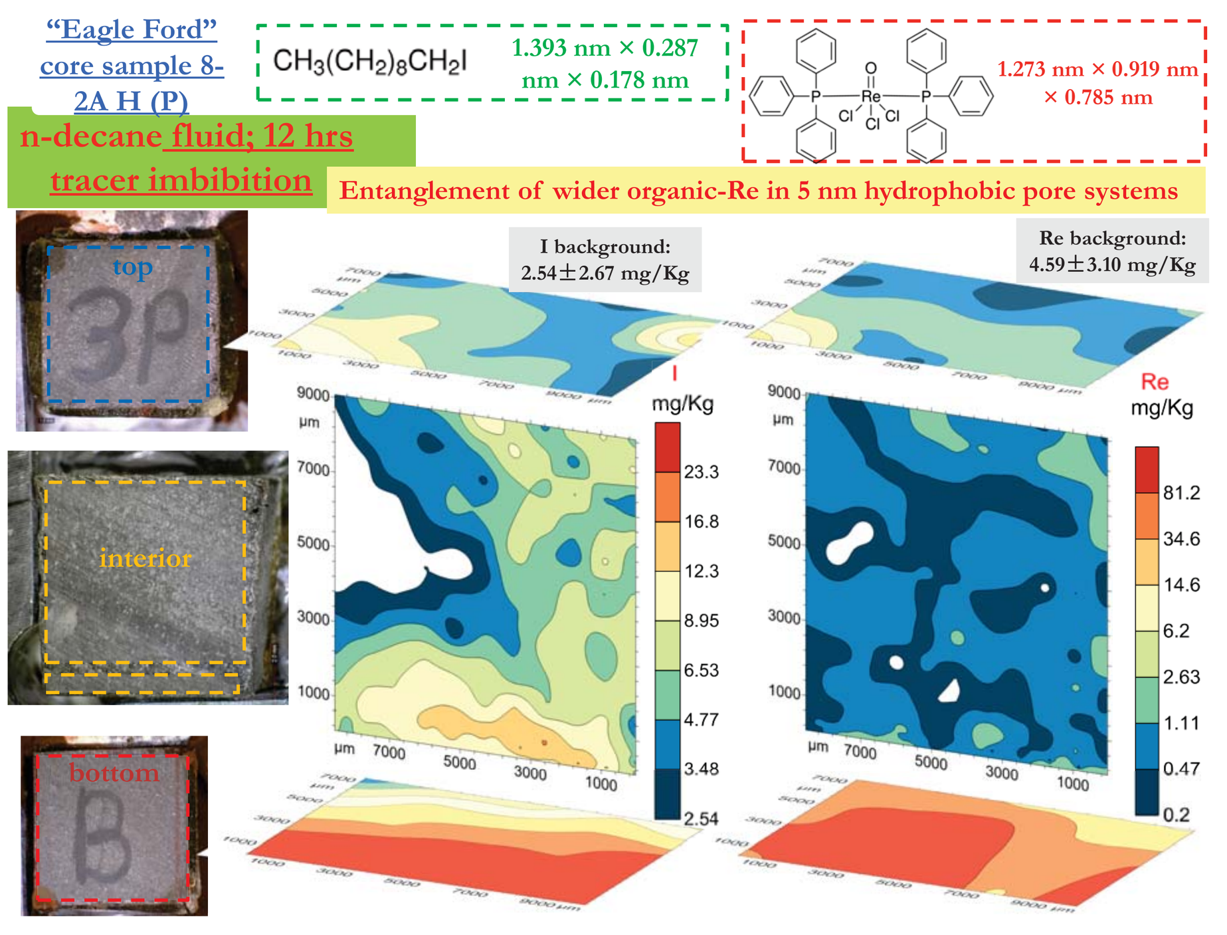

Diffusivity: Liquid Tracer Diffusion

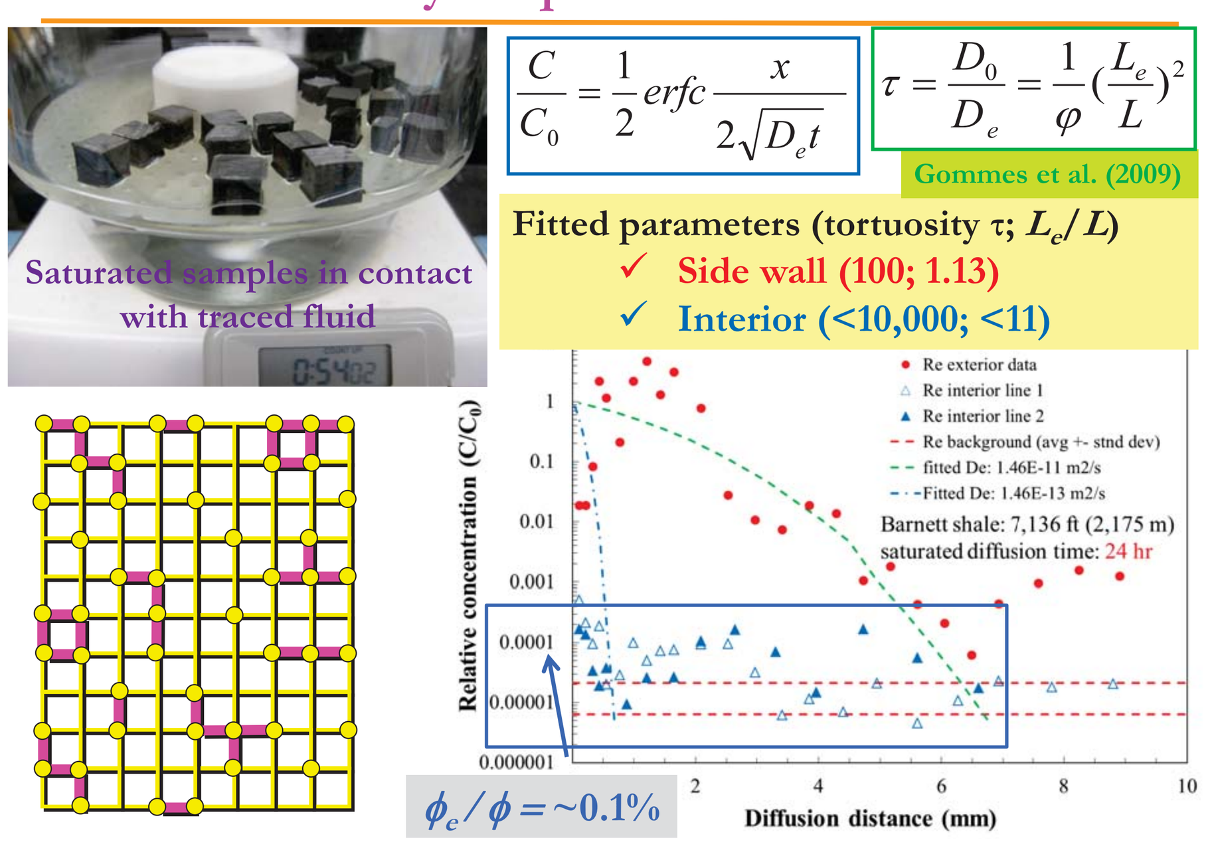

Approach: Liquid Pycnometry

Large-sized samples: Vacuum saturation with different fluids

Polar: DI water; API brine

Non-polar: n-decane:toluene=2:1 (1:1; 10:1)

Bi-polar: tetrahydrofuran

Liquid pycnometry: originally designed for SOLID samples

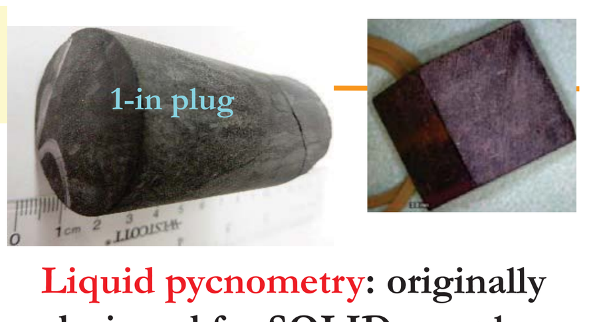

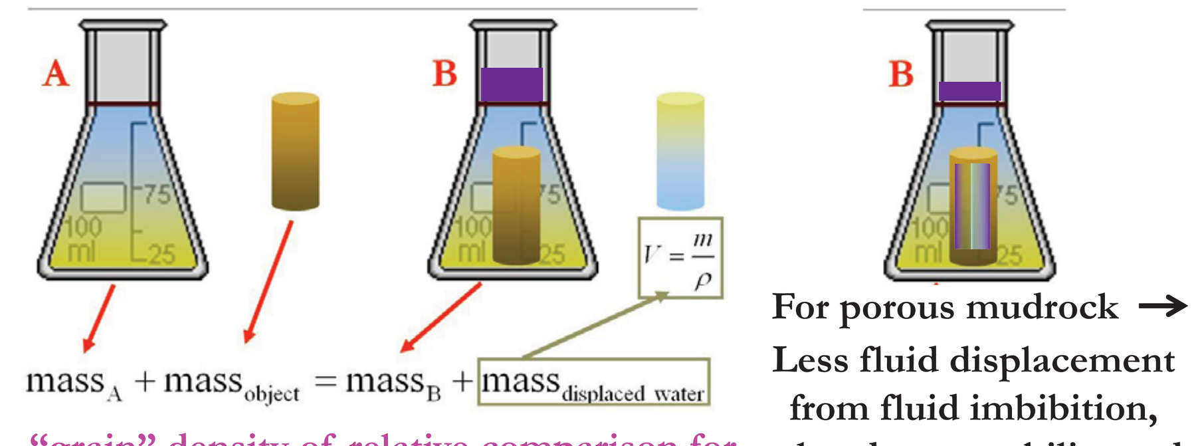

"grain" density of relative comparison for sample size-dependent effective porosity

For porous mudrock → Less fluid displacement from fluid imbibition, related to wettability and connectivity

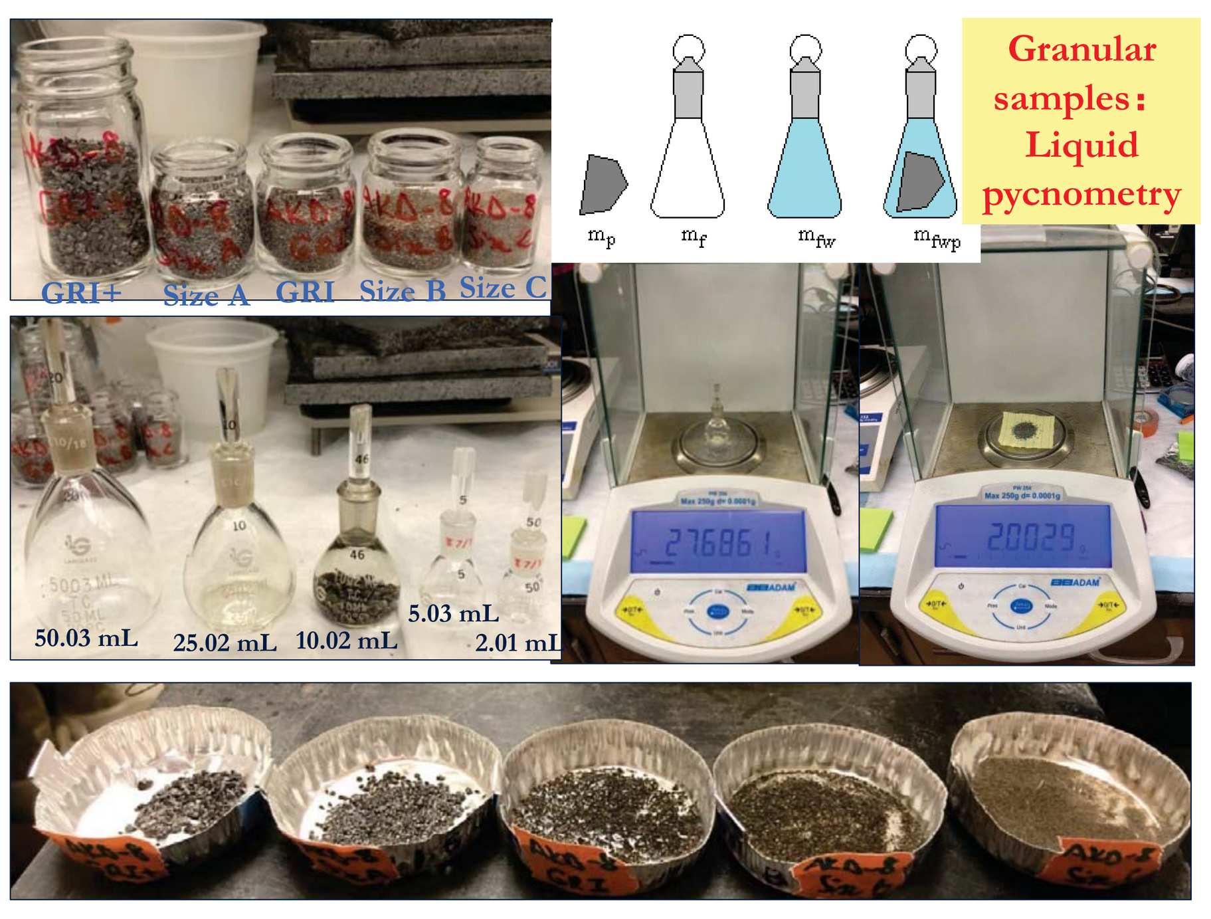

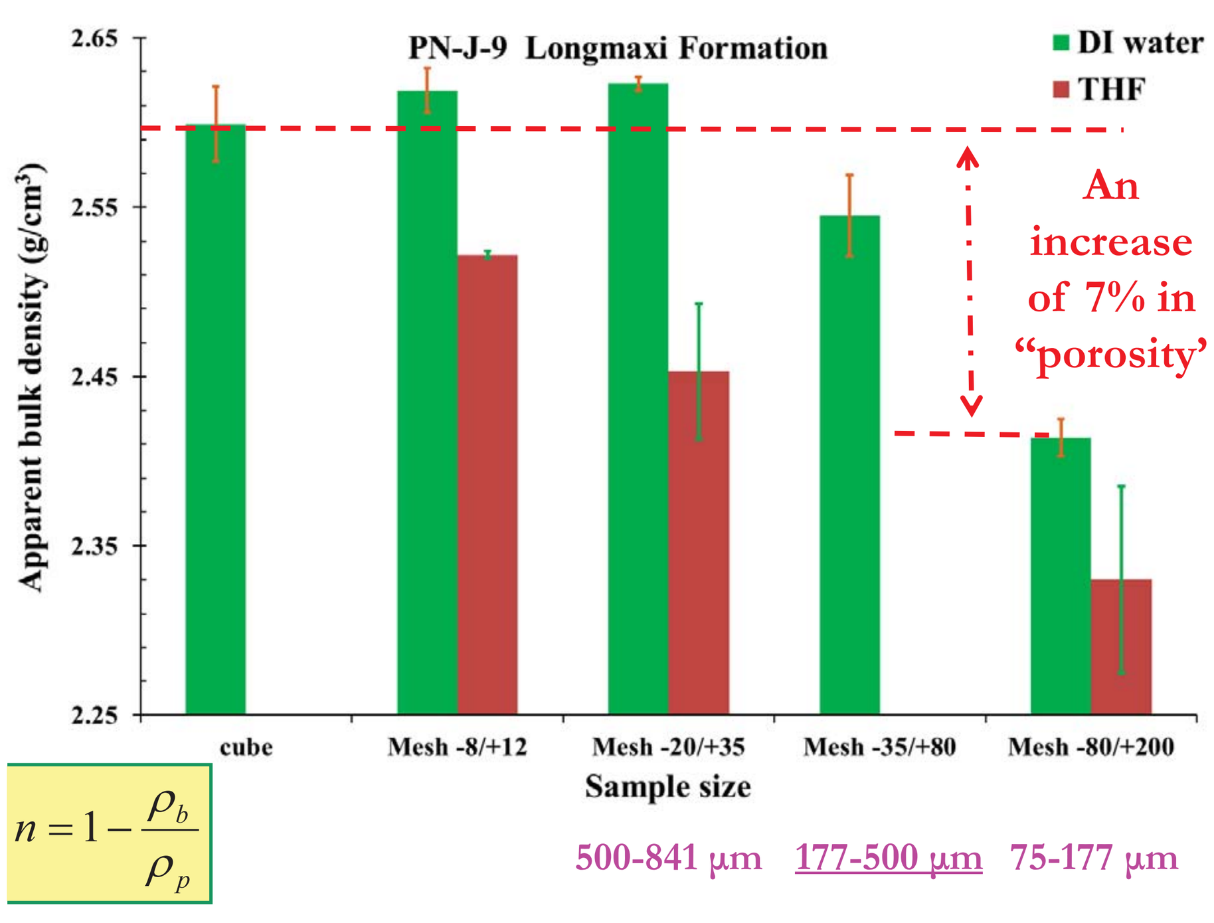

$$n = 1 - \frac{\rho_b}{\rho_p}$$

500-841 μm 177-500 μm 75-177 μm

Approach: Small Angle Neutron Scattering

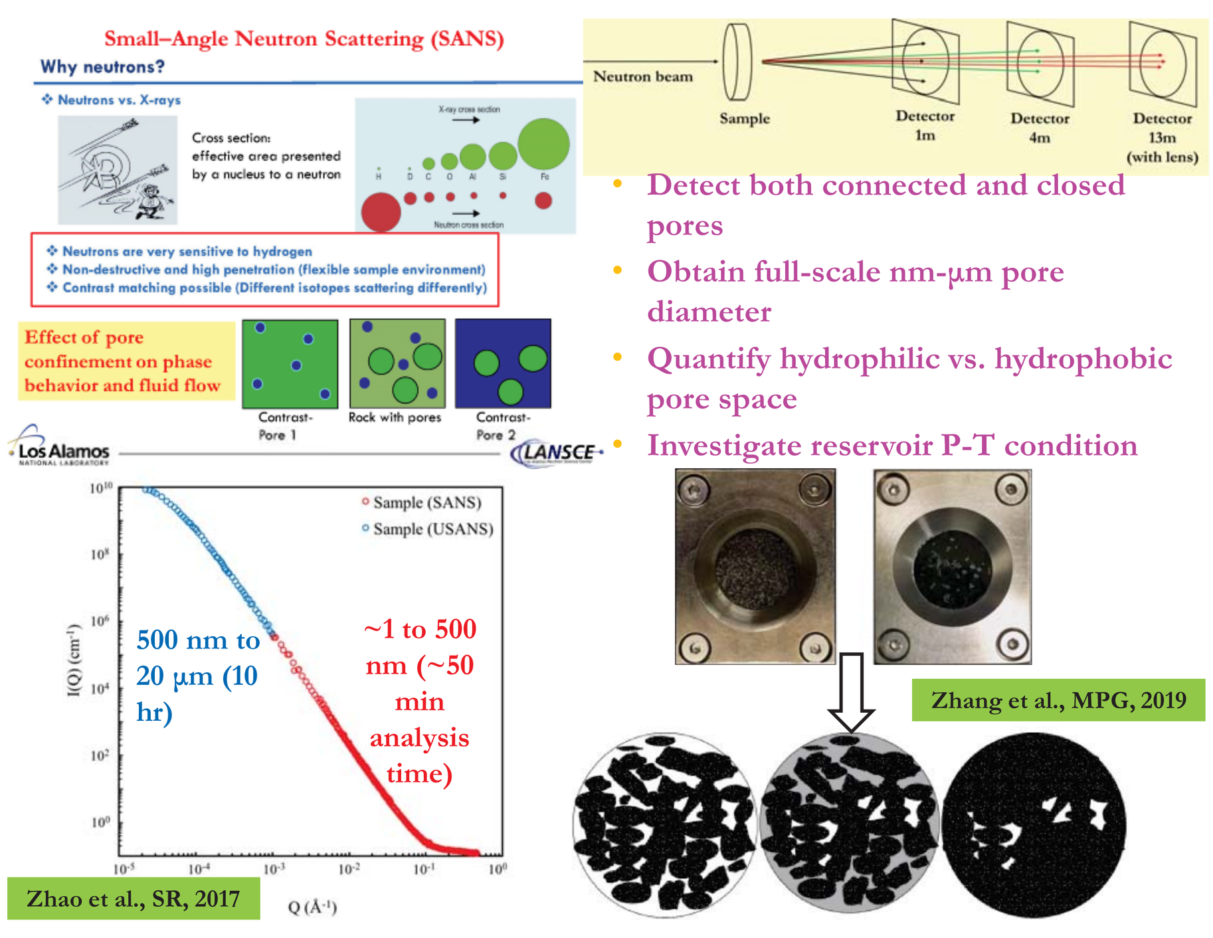

- Detect both connected and closed pores
- Obtain full-scale nm-μm pore diameter
- Quantify hydrophilic vs. hydrophobic pore space
- Investigate reservoir P-T condition

Zhang et al., MPG, 2019

(U)SANS: Fluid-Wettable Pore Space

Zhang et al., AAPG, 2018 (under review)

	Utica (Late Ordovician) (R_0<0.5%)	Utica (R_0=0.82%)	Middle Bakken (late Devonian)
Porosity Results(%)	Sample 1	Sample 2	Sample 3
Total	11.4	7.83	9.28
Hydrophyllic	7.04	2.7	7.16
Hydrophobic	4.92	2.58	2.32
MICP Accessible	2.12	0.79	3.71

Upper Bakken	Formation	TOC	MICP (1cm cube)	(U)SANS (grains: 177-500 μm) (1.1 nm – 20 μm)	MICP (grains: 177-500 μm) (3.4nm - 50 μm)	MICP (grains: 177-500 μm) (3.4 nm - 10 um)
Sample #4	Bakken	13.7wt.%	2.29%	11.69%	13.20%	11.10%

Summary

Unique Dual-Connectivity Zones of Shale: Multiple Evidence

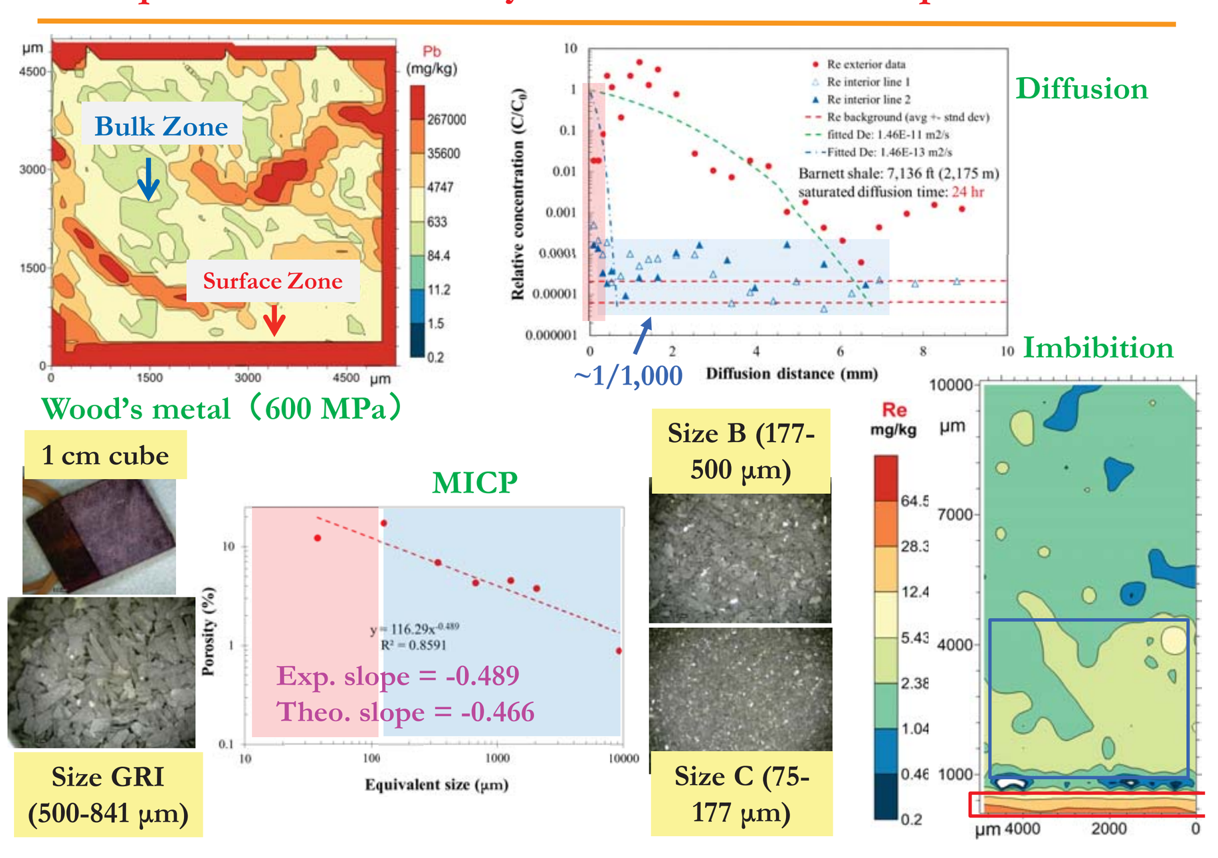

Edge-accessible Effective Porosity

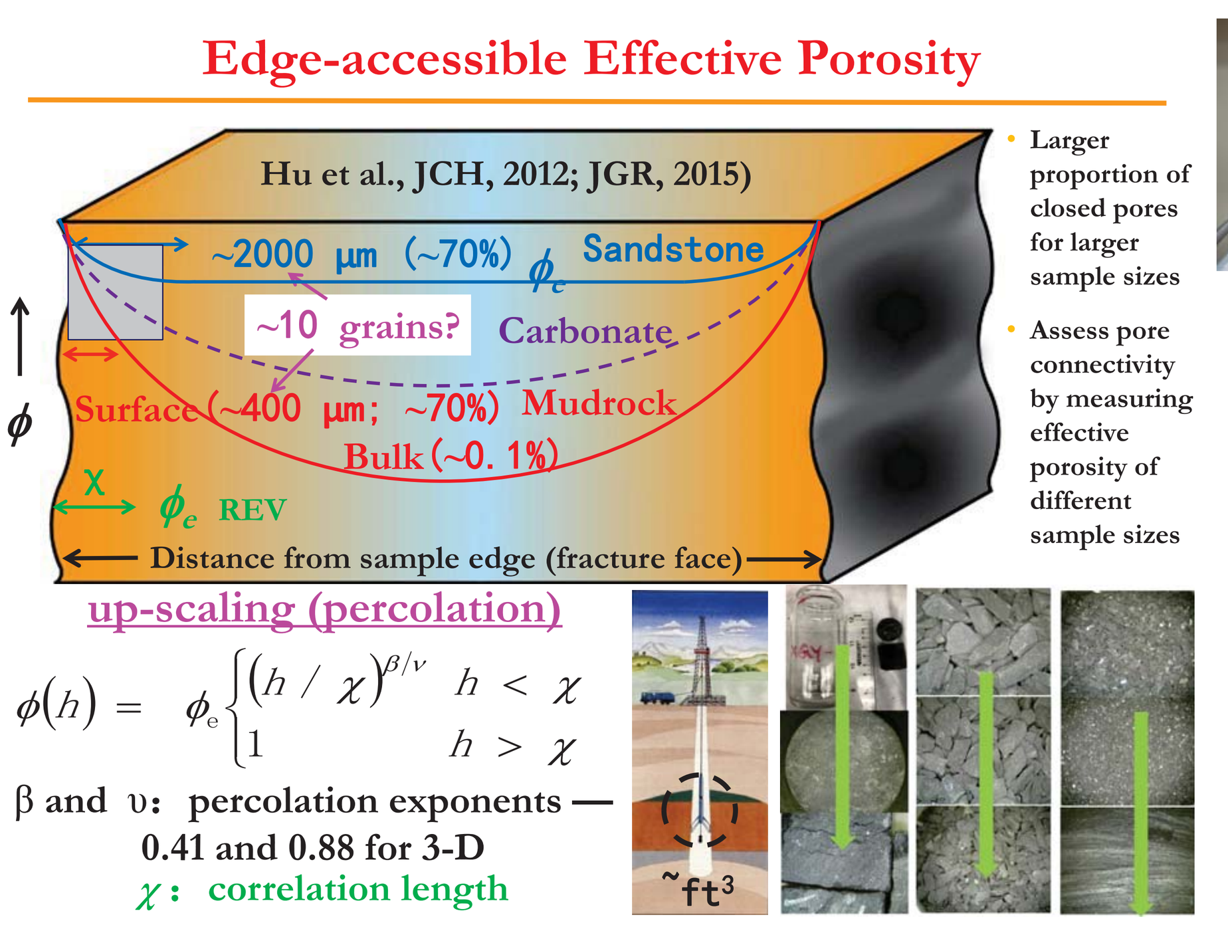

- Larger proportion of closed pores for larger sample sizes
- Assess pore connectivity by measuring effective porosity of different sample sizes

up-scaling (percolation)

$$\phi(h) = \phi_c \begin{cases} (h/\chi)^{\beta/\nu} & h < \chi \\ 1 & h > \chi \end{cases}$$

β and ν: percolation exponents — 0.41 and 0.88 for 3-D

χ: correlation length

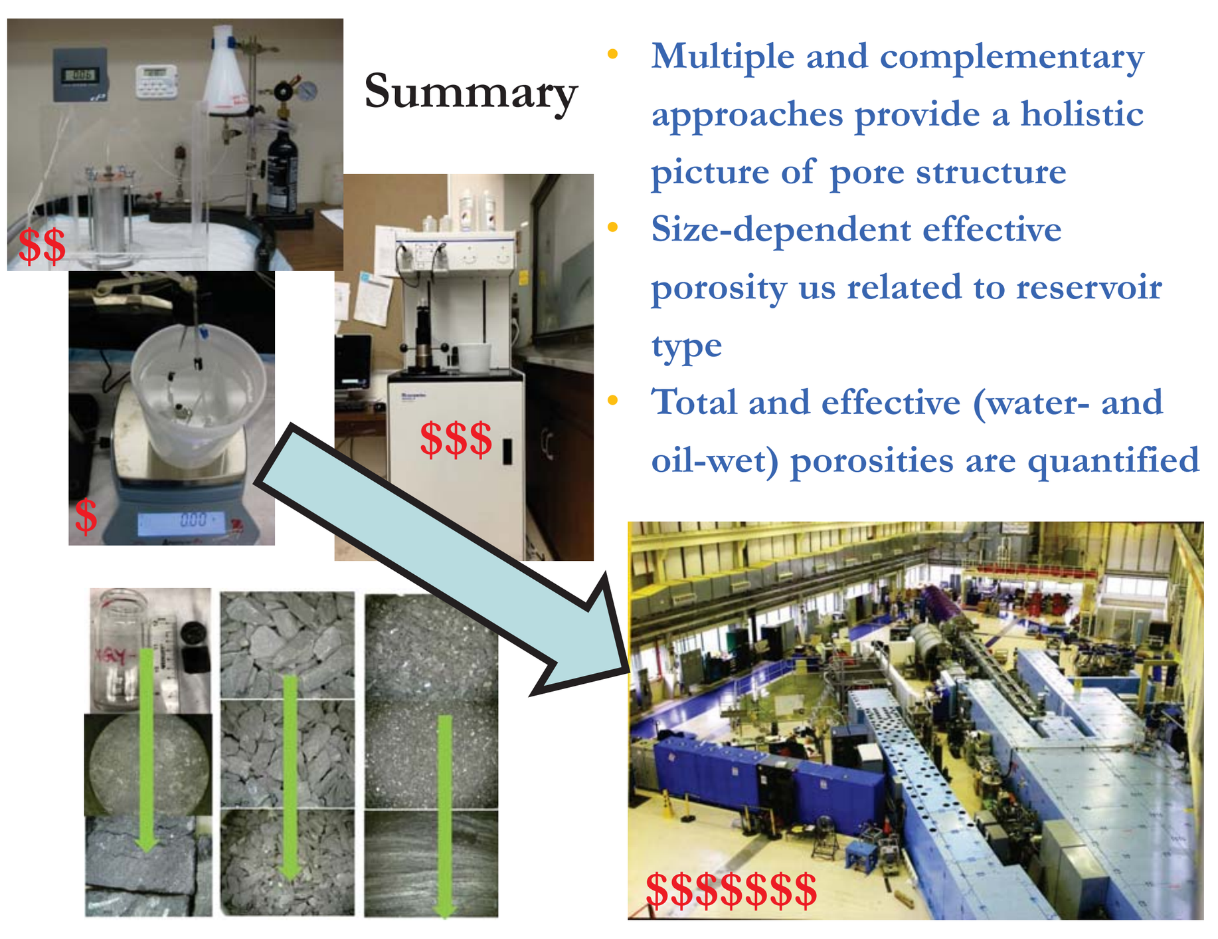

- Multiple and complementary approaches provide a holistic picture of pore structure
- Size-dependent effective porosity us related to reservoir type
- Total and effective (water- and oil-wet) porosities are quantified

References

- Gao, Z.Y., and Q.H. Hu. 2013. Estimating permeability using median pore-throat radius obtained from mercury intrusion porosimetry. *Journal of Geophysics and Engineering*, 10, 025014.
- Gao, Z.Y., and Q.H. Hu. 2016. Wettability of Mississippian Barnett samples at different depths: Investigations from directional spontaneous imbibition. *AAPG Bulletin*, 100(1): 101–114.
- Gao, Z.Y., and Q.H. Hu. 2018. Pore structure and spontaneous imbibition of marine and continental shales in China. *AAPG Bulletin*, 102(10): 1941–1961.
- Hu, Q.H., T.J. Kneafsey, J.S.Y. Wang, L. Tomutsa, and J.J. Roberts. 2004. Characterizing unsaturated diffusion in porous tuff gravels. *Vadose Zone Journal*, 3(4): 1425–1438.
- Hu, Q.H., R.P. Ewing, and S. Dultz. 2012. Pore connectivity in natural rock. *Journal of Contaminant Hydrology*, 133: 76–83.
- Hu, Q.H., and X.L. Mao. 2012. Applications of laser ablation-inductively coupled plasma-mass spectrometry in studying chemical diffusion, sorption, and transport in natural rock. *Geochemical Journal*, 46(5): 459–475.
- Hu, Q.H., R.P. Ewing, and H.D. Rowe. 2015. Low nanopore connectivity limits gas production in Barnett Formation. *Journal of Geophysical Research – Solid Earth*, 120(12): 8073–8087.
- Hu, Q.H., H. Liu, R. Yang, Y.X. Zhang, G. Kibria, S. Sahi, N. Alatrash, F.M. MacDonnell, and W. Chen. 2017. Applying molecular and nanoparticle tracers to study wettability and connectivity of Longmaxi Formation in southern China. *Journal of Nanoscience and Nanotechnology*, 17: 6284–6295.
- Hu, Q.H., Y.X. Zhang, X.H. Meng，Z. Li, Z.H. Xie, and M.W. Li. 2017. Characterization of multiple micro-nano pore networks in shale oil reservoirs of Paleogene Shahejie Formation in Dongying Sag of Bohai Bay Basin, East China. *Petroleum Exploration and Development*, 44(5): 720–730.
- Hu, Q.H., W. Zhou, P. Huggins, and W.L. Chen. 2018. Pore structure and fluid uptake of the Goddard Shale Formation in Southeastern Oklahoma, USA. *Geofluids*, Article ID 5381735.
- Zhao, J.H., Z.J. Jin, Q.H. Hu, Z.K. Jin, T.J. Barber, Y.X. Zhang, and M.K. Bleuel. 2017. Integrating SANS and fluid-invasion methods to characterize pore structure of typical American shale oil reservoirs. *Scientific Reports*, 7: 15413.